January 2012

Structure and Dynamics of the p53 Transactivation Domain Binding to MDM2 and RPA70

Anne Terese Powell
University of South Florida, annirese@hotmail.com

Structure and Dynamics of the p53 Transactivation Domain Binding to MDM2 and RPA70

By

Anne Terese Powell

A thesis submitted in partial fulfillment of the requirements for the degree of
Masters of Science in Biology,
Department of Cell Biology, Microbiology, and Molecular Biology,
College of Arts and Sciences,
University of South Florida

Major Professor: Gary Daughdrill, Ph.D.
Kristina Schmidt, Ph.D.
Stanley Stevens, Ph.D.
Jiandong Chen, Ph.D.

Date of Approval:
March 22, 2012

Keywords: Nuclear Magnetic Resonance, Isothermal Titration Calorimetry, Thermodynamics, Intrinsically Disordered Proteins, Polymorphism

Dedication

I would like to dedicate this work to my late aunt, Mary Ann Long. She always encouraged me to be my best. Her memory is a driving force in my life to help those affected by cancer. This work is also dedicated to my mother, Elizabeth Johnston. Her constant pursuit of knowledge and her curiosity are infectious. She has taught me through example that anything is possible. This work is also dedicated to my father, Gary Pine. He has the strongest work ethic of any man that I have ever met. I try to emulate his resolve not only to work, but to do the best work.

Acknowledgements

I would like to thank Dr. Gary Daughdrill for his patience and guidance. I am grateful for the time and direction from my committee members. Dr. Kristina Schmidt was invaluable during my graduate experience. I would like to thank Dr. Hongwei Wu, Wade Borcherds and Katie Mishall for their help and contribution to this work. As an undergraduate researcher, Katie assisted with most of the RPA70 experiments. Most of all I would like to thank my husband Chase. His support, encouragement, and understanding were priceless. Lastly, I would like to say thank you to my children for their sacrifice of time.

Table of Contents

List of Tables

List of Figures

Abstract

The tumor suppressor protein, p53, is mutated or dysregulated in nearly all human cancers(1). The amino terminal domains are essential for transcriptional activation in stressed cells and play a vital role in cell cycle regulation, apoptosis and senescence. The transactivation (TAD) and proline rich domains in this region are dynamic and intrinsically disordered; lacking stable secondary or tertiary structure. This region contains multiple binding sites; arguably, the most significant of these is for p53's negative regulator, the E3 ligase, MDM2. An important, but less understood interaction involving the single stranded DNA binding protein, RPA70A, is hypothesized to be involved in maintaining genome integrity(2-4). Additionally, the amino terminus contains an important single nucleotide polymorphism that has demonstrated different affinity for MDM2 and is of significant biological importance in the induction of apoptosis (5). Isothermal titration calorimetry (ITC) and nuclear magnetic resonance (NMR) spectroscopy were employed to investigate how the thermodynamics and the inherent flexibility of the amino terminus of p53 play a role in complex formation with the MDM2 or RPA70 proteins. Understanding the structure, dynamics, and function of p53 is paramount in the fight against cancer.

Chapter 1: The History, Structure, and Binding Partners of p53

The History of p53

The discovery of p53. A connection between oncogenic transformation and viral infection, exemplified by the human papilloma virus (HPV) and Epstein-Barr virus, had been established by the mid 1970's(6). In the pursuit to identify the middle T antigen of the SV40 virus a protein that was approximately 55 kilo Daltons (kDa) was immunoprecipitated; it was soon realized that it was not a viral protein, but was encoded by the host cell(6). Interestingly, the middle T antigen of the SV40 virus does not exist, but in looking for it they found the p53 protein. The existence of the p53 protein was first published in 1979 as a cellular protein using two approaches, virological and immunological; at the time it was not known that both approaches were describing the same protein (6-12). In 1983, Crawford published that the protein identified in both approaches was the same and named it p53; the research field of p53 was born (13).

There was a fundamental shift about causation in cancer in the early 1980's going from a viral model of pathogenesis to an oncogenic model; the discovery of tumor suppressor genes would come in the late 1980's (6). The p53 protein was originally believed to be an oncoprotein for a multitude of reasons. It was implicated in cell proliferation, associated with the activated oncogene Ha-

Ras, and demonstrated nuclear localization and accumulation in cancer cells but was not present in untransformed cells (14-23).

These initial observations are consistent with p53 function, but were misinterpreted because the function of p53 was not yet understood. When cells are exposed to stress p53 is activated and accumulates within the nucleus. The wildtype p53 had not been define and the p53 protein was a truncated or mutant form in mouse cancer cells leading to functional inactivation of p53 (24). It was shown that families who have a condition called Li-Fraumeni syndrome, which is associated with a high risk for multiple cancers, often have a germ line mutation in p53 (25, 26). It was shown that the p53 protein had antiproliferative properties, and was often deleted or mutated in human cancer (6, 24, 27, 28). The p53 gene encoded a tumor suppressor protein (29, 30).

The function of p53. The p53 protein is ubiquitously expressed and maintained at low levels under normal cellular conditions (31-33). The p53 pathway is activated when the cell is exposed to different stresses and activation leads to growth arrest, DNA repair, senescence or apoptosis (1, 33-35). The function of p53 is to maintain genome integrity(34). If p53's function is altered through, mutation, deletion of the gene or through dysregulation cancer is almost inevitable. For this reason, p53 is one of the most significant targets in cancer research.

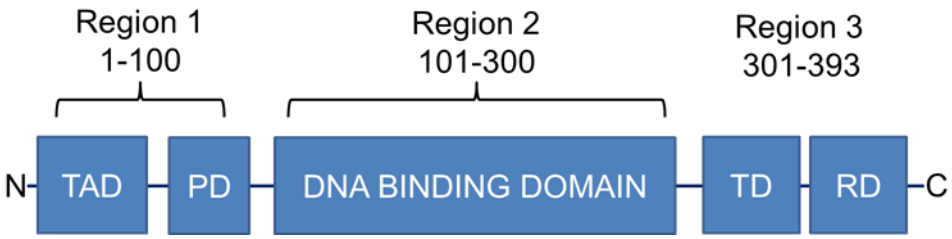

Figure 1. The domain structure of p53 protein. The transactivation domain (TAD), Proline Rich Domain (PD), the DNA Binding Domain, the Tetramerization domain (TD), and Regulatory Domain (RD) are shown in blue with the associated regions of the protein demonstrated above the domains.

The p53 Protein

The domains of p53. The human p53 protein has 393 amino acids and contains five domains that can be divided into three distinct regions; region 1 contains two amino terminal domains, region 2 is the middle DNA binding domain, and region 3 contains two carboxyl terminal domains (figure 1). The first region, residues 1-100, contains the transactivation domain and proline rich domain. This region contains the binding site for p53's negative regulator, the E3 ligase, MDM2. Additionally, this region contains an important functional polymorphism at position 72 that encodes either a proline or an arginine. The second region encompassing residues 101-300 contains the DNA binding domain. The DNA binding domain is where most of the mutations occur that lead to oncogenic transformation (36). The third region at the carboxyl terminus, residues 301-393, contains the tetramerization and regulatory domain respectively.

p53 is an Intrinsically Disordered Protein. Historically it was thought that a rigid three dimensional structure was necessary for biological function, but the classic structure-to-function paradigm is now changing (37). In the past

decade, the view that rigid protein structure gives rise to its biological function has been evolving due to the discovery that multiple systems lack tertiary structure and that absence of rigid structure is important for their function. These advances have led to the discovery of a new family proteins that do not form compact rigid structure under normal physiological conditions (38). These partially or completely disordered proteins are called intrinsically disordered proteins (IDPs) (37, 39-43).

Intrinsically disordered proteins are common in nature (44). Proteomes of highly complex organisms contain higher numbers of IDPs compared with less complex organisms(39). This is thought to be a result of the increased need for cell signaling and gene regulation in more complex organisms(45). IDPs have high specificity and low affinity for their binding partners and this is important in cell regulation allowing these interactions to be easily reversed (44-46). IDPs are overrepresented in protein families that are involved in transcription, translation, signal transduction, and cell cycle regulation (45, 47). Another characteristic that is unique to IDPs is the ability to fold in the presence of a ligand or binding partner. This mechanism is called coupled folding binding, and can be referred to as a disorder-to-order transition (39, 44-46).

The intrinsically disordered protein family is characterized as having no compact globular core, extended structure, and sample a dynamic range of conformations under normal physiological conditions (39, 44-49). The ability to sample a wide range of conformations can be a functional advantage. For instance, a single disordered protein can bind to different proteins in unique

conformations with high specificity and low affinity (44-46, 50). The ability to sample numerous conformations allows for binding with many distinctive protein partners or ligands (44-47).

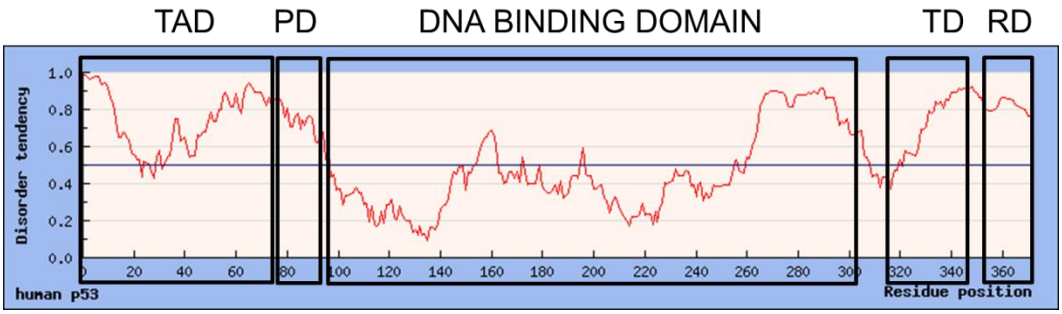

Figure 2. The disorder predictor IUPred was used to diagram of the p53 full length protein. This disorder predictor uses amino acid composition and energy content information to determine if a give sequence will contain intrinsic disorder (49, 50). Disorder tend tendency values above 0.5 are predicted to be disordered and values below 0.5 are predicted to contain secondary and tertiary structure. The TAD, PD, DNA Binding Domain, TD, and RD domains are outlined in black. The residue position is listed on the X axis.

The p53 protein is an intrinsically disordered protein (40, 51). In monomeric p53 the amino terminal and carboxyl terminal do not form stable secondary structure; only the DNA binding domain having established secondary and tertiary structure (figure 2). The tetramerization domain will form stable structure in the tetrameric p53. The crystal structure of the DNA binding domain was first published in 1994 (52). The intrinsic disorder inherent to both termini of the protein would aid in p53's important role in cell cycle regulation (53). Additionally, p53 goes through a disorder-to-order transition when binding the single stranded DNA binding protein, RPA70 or its negative regulator, MDM2 (3).

The p53 binding partner RPA70. The single stranded DNA binding protein, replication protein A is composed of 3 subunits; a 14kDa, a 32kDa, and

70kDa subunits (54, 55). The 70 kDa subunit of RPA70 is essential in DNA replication and chromosomal stability (54-56). The p53 transactivation domain (TAD) binds the RPA70 protein and it has been shown that single stranded DNA and p53 compete for binding with RPA70 (3, 57-60). The competition between single stranded DNA and the p53 protein is hypothesized to be important in the response to DNA damage and potentially provides a pool of p53 to respond immediately after damage occurs (3, 4, 60).

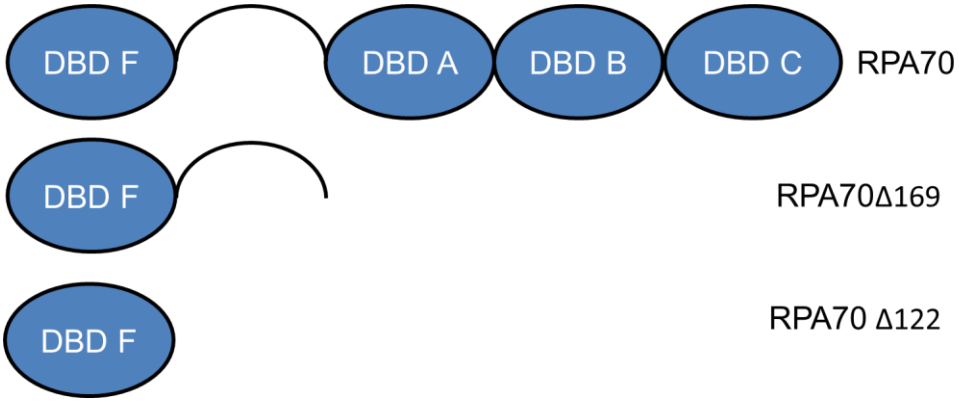

Figure 3. The RPA70 protein domains. The full length protein is shown at the top followed by the deletion mutants created for experiments used in this work. The full length protein contains DNA binding domain F (DBDF), then a flexible linker that connects to DNA Binding Domain A (DBDA), DNA Binding Domain B (DBDB), DNA Binding Domain C (DBDC).

The domain structure of RPA70 is shown in figure 3. The tumor suppressor protein p53 binds the basic cleft on the amino terminal end of RPA70 in the DNA binding domain F (DBDF) and at the carboxyl terminal end in the DNA binding domain C (DBDC) of RPA70 (3). Deletion mutant analysis has been employed to investigate DBDF binding to p53 and to single stranded DNA (3).

Regulation of p53 by the E3 ligase, MDM2. The Murine Double Minute 2 (MDM2) oncoprotein was first identified when it was found to induce cancer transformation in a mouse cell line and further reports showed its involvement in human sarcomas in the early 1990's (61-63). It was also shown that MDM2 formed a complex with p53 and inhibited p53 transactivation (62). MDM2 not only binds to p53 and inhibits p53 transactivation it is also an ubiquitin E3 ligase activity that targets p53 for degradation by ubiquitinating the carboxyl terminus of p53. Additionally, activated p53 induces the transcription of MDM2; this creates and auto-regulatory feedback (figure 4).

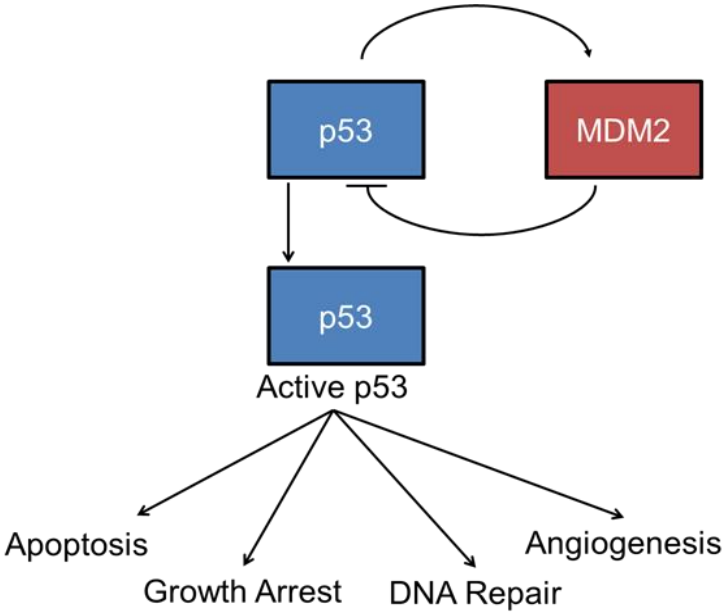

Figure 4. The p53 and MDM2 autoregulatory negative feedback loop. Activation of p53 leads to angiogenesis, growth arrest, DNA repair, or apoptosis.

The polymorphism at codon 72 in the p53 protein.

History and functional differences of the polymorphism. The arginine/proline polymorphism at codon 72 was first reported in 1990 (64). Following this discovery, Thomas et. al. reported that both variants could be considered wild type based on DNA sequence specific binding, but noted a difference in transcriptional activation and apoptotic induction between the

polymorphs (65). This polymorphism occurs within the proline rich domain and accounts for one of the PXXP motifs indicating that it may alter protein-protein interactions (66). It has been shown at the cellular level to have differential implications in cancer predisposition, age of onset, and patient survival (5, 66-72). The preeminence of the data points to a substantial dissimilarity in apoptotic potential between the two alleles; with the arginine allele causing stronger induction of apoptosis as opposed to the proline allele (5, 72). Although a structural difference has been reported through proteolytic digest and differential shifts on SDS-PAGE gels, a detailed structural explanation is still lacking (66).

At a cellular level, the p53 72R variant binds MDM2 with a higher affinity than 72P allele as determined by an immunoprecipitation assay (5, 66). The difference in binding affinity may be due to differences between the structure and dynamics of the allelic protein ensembles. Alternatively, another protein binding site within the amino terminal domain of p53 could be affecting the MDM2 binding affinity; the second site has been preliminarily shown to bind to MDM2 with lower affinity than the primary MDM2 binding site (73). It is reasonable to assume that the basic nature of the arginine at position 72 alters the electrostatic interactions within the transactivation and proline rich domains giving rise to the differential affinity of the variants with MDM2 and ultimately influencing biological function of the p53 protein.

Chapter 2: Materials, Methods, and Experimental Design

Creation of constructs

The Pet28a vector was used for the p53 constructs p53Δ74_72R, p53Δ91_72P, the Pet28d vector was used for RPA70Δ169, RPA70Δ130 and were created in the lab previously (3). The pGex6P2 MDM2 (17-125) construct was ordered from GeneArt (Invitrogen, Grand Island, NY). The following constructs were made with a QuikChange II Site-Directed Mutagenesis Kit (Stratagene, Wilmington, DE), p53Δ74_D21E, _K24E, _K24A, _K24Q, _K24N, p53Δ91_72P_E28C, pGex6P2 p53Δ91_72R_E28C, RPAΔ129, Δ128, Δ127, Δ126, Δ125, Δ124, Δ123, Δ122, Δ121, Δ120, and RPAΔ300_L280F, RPAΔ400_L280F, RPAΔ400_L280F. The p53Δ91_72R construct was ordered from GeneArt (Invitrogen, Grand Island, NY) and sub cloned into the pGex6P2 vector using the restriction enzymes EcoR1 and BamH1 (New England Biolabs, Ipswich, MA). All constructs were transformed into NEB5α *E. coli* cells. One nanogram of plasmid DNA was mixed with 50μL of competent cells and incubated on ice for 30 minutes, heat shocked for 45 seconds, followed by incubation on ice for 5 minutes. SOC media, 950 microliters, was added to the mixture and was incubated at 37°C for 1 hour with 225 rpms in a shaker incubator. The mixture was then plated on a plate with the appropriate antibiotic (ampicillin or kanamycin) and incubated 16-18 hours at 37°C. Single colonies were picked and grown overnight in NZY broth with the appropriate antibiotic.

The next morning the cultures were spun down at 4°C at 5400xg for 10 minutes. A Qiagen miniprep kit would be used to extract the plasmid DNA from the cultures (Valencia, CA). The sequences were confirmed by MWG Operon (Huntsville, AL) and sequence analysis using Geneious software.

Protein Expression

All the protein constructs used in this study were transformed into BL21 (DE3) competent *E. coli* (Invitrogen). One nanogram of plasmid DNA was mixed with 20µL of competent cells and incubated on ice for five minutes, placed at 42° C for 30 seconds, followed by incubation on ice for 2 minutes. Eighty microliters of SOC media was added to the mixture followed by incubation at 37°C for 1 hour with shaking at 225 rpms. The mixture was then plated on LB agar with the appropriate antibiotic (ampicillin or kanamycin) and incubated 16-18 hours at 37°C.

Minimal media was made and one colony was picked to inoculate 50ml overnight cultures (appendix 1). The controls for the inoculation of overnight cultures were as follows. Two milliliters of culture were removed and placed in a sterile test tube. One gram on ammonium chloride was added to each liter of sterilized media. Next two milliliters were removed from the nitrogen containing media and added to a sterile test tube. Two grams of glucose were then added and mixed with the each of the sterile liters of media. Two milliliters of media was removed and added to a third sterilized test tube. Control tube 1 and 2 had bacteria colony added; the third tube was a sterility control and did not get inoculated with a colony. For isotopically labeled samples, 1 g/l of ^{15}N-labeled

ammonium chloride and/or 2g/l ^{13}C-labeled glucose were added in the place of nitrogen and carbon sources (Cambridge Isotopes, Andover, MA).The next morning the 50ml overnight cultures were used to inoculate two liters of media. The cultures were induced at an optical density (A_{600}) of 0.6-0.8 via a T7 driven promoter using 1mM of Isopropyl β-D-1-thiogalactopyranoside (IPTG). The RPA70 constructs and the MDM2 constructs were grown for 4 hours. The p53 constructs were grown for 6 hours. The RPA70 and p53 constructs were induced at 37°C and the MDM2 protein was induced at 25°C to reduce inclusion body formation. The cultures were pelleted after induction by spinning at 8,000rpm at 4°C. The pellets were stored at -80°C until purification.

Protein Purification

Purification of p53. The p53 culture pellets were thawed on ice and suspended in 50mM sodium phosphate monobasic, 300mM sodium chloride, 10mM imidazole, and 0.02% sodium azide pH 8. The cells were lysed by two passes through a French press with 1200 psi. The supernatant was collected and cellular debris was spun out in a centrifuge at 38,360xg at 4°C for 1 hour. The supernatant was filtered and run through a nickel resin (BioRAD) column on an AKTA fast protein liquid chromatography (FPLC) unit (GE Healthcare, Pittsburgh, PA). Protein binding and elution to the nickel resin was monitored using an

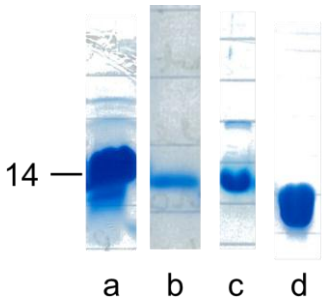

Figure 5. SDS-PAGE gel of purified p53 proteins. A, B, C, and D shown above are p53Δ74_72R, canine p53TAD, p53Δ74_72R_K24N, p53Δ74_72R_P27A respectively. All proteins ran at approximately 14 kDa.

ultraviolet spectrometer with the wavelength set at 280 nm. The apparent mass of fractions corresponding to eluted protein was determined using sodium dodecyl sulfate polyacrylamide gel electrophoresis (SDS PAGE) (figure 5). Fractions corresponding to p53TAD were combined and dialyzed 1000 fold into gel filtration buffer (50mM sodium phosphate monobasic, 300mM sodium chloride, 1mM EDTA, and 0.02% sodium azide pH 7). The protein was then concentrated to a volume of ~12millilters and the histidine tag was cleaved in two hours at room temperature with gentle rocking using a thrombin cleavage kit (Sigma Aldrich, St. Louis, MO). A pre-cleave and post cleave sample is saved for SDS analysis to confirm cleavage of the tag. The sample volume is then reduced to approximately 6mls using a centricon centrifugal concentrator with a 3000 molecular weight cut off (MWCO) at 4,000xg at 4°C and run on a size exclusion column (SEC) at one milliliter per minute flow rate. The relevant fractions were collected and confirmed on an SDS PAGE gel and dialyzed into the appropriate buffer. The NMR buffer contained 50mM sodium phosphate monobasic, 50mM sodium chloride, 1mM EDTA, and 0.02% sodium azide pH 6.8 for p53 studies. The p53 and RPA70 binding studies used 50mM sodium phosphate monobasic, 50mM sodium chloride, 1mM EDTA, 2mM DTT, and 0.02% sodium azide pH 6.5. The NMR buffer contained 50mM sodium phosphate monobasic, 100mM sodium chloride, 1mM EDTA, 5mM DTT, and 0.02% sodium azide pH 7 for p53 and MDM2 binding studies. The ITC buffer for p53 and MDM2 was 50mM sodium phosphate monobasic, 100mM sodium chloride, 1mM EDTA, 8mM βME and 0.02% sodium azide pH 7.

Purification of RPA70. RPA70 deletion mutants RPAΔ122 and RPAΔ169 were used for NMR experiments. Both were purified with the same protocol. The RPA70 culture pellets were thawed on ice and suspended in 30mM HEPES, 0.25mM EDTA, 0.25% w/v inositol, 0.01% w/v IGEPAL, 50mM KCl, and 1mM DTT. The cells were lysed by two passes through a French press with 1200 psi. The supernatant was collected and cellular debris was spun out in a centrifuge at 38,360xg at 4°C for 1 hour. The supernatant was filtered and run on a fast flow Affigel blue resin column (BioRAD) column on an AKTA fast protein liquid chromatography (FPLC) unit (GE Healthcare, Pittsburgh, PA). Protein binding and elution to the Affigel blue resin was monitored using an ultraviolet spectrometer with the wavelength set at 280 nm. The apparent mass of fractions corresponding to eluted protein was determined using SDS PAGE (figure 6). The fractions containing the protein were pooled and dialyzed into gel filtration buffer (50mM sodium phosphate monobasic, 300mM sodium chloride, 1mM EDTA, 2mM DTT, and 0.02% sodium azide pH 7). The protein was concentrated and brought down to a volume of approximately 6-8 mls and run on a size exclusion column (SEC) at one milliliter per minute flow rate. The fractions were run on a 15% SDS PAGE gel and the fractions containing the protein were dialyzed into 50mM sodium phosphate

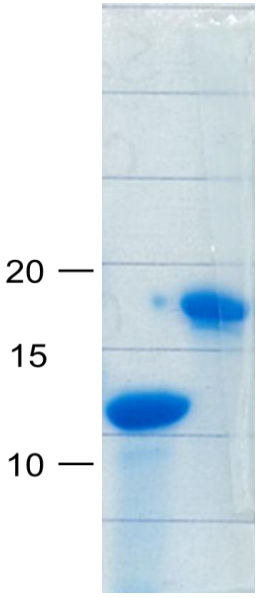

Figure 6. SDS PAGE gel with RPA70 purified proteins; RPAΔ122 is on the left and RPAΔ169 is on the right. The molecular weight markers are shown on the left.

monobasic, 50mM sodium chloride, 1mM EDTA, 2mM DTT, and 0.02% sodium azide pH 6.5 and concentrated down to .3mM to .45mM for NMR studies.

Purification of MDM2. The MDM2 culture pellets were thawed on ice and suspended in 50mM Tris•HCl, 300mM sodium chloride, 2.5mM EDTA, 1mM DTT, and 0.02% sodium azide pH 7.4. The cells were lysed by two passes through a French press with 1200 psi. The supernatant was collected and cellular debris was spun out in a centrifuge at 38,360xg at 4°C for 1 hour. The supernatant was filtered and run through a GST resin column on an AKTA fast protein liquid chromatography (FPLC) unit (GE Healthcare, Pittsburgh, PA). Protein binding and elution to the GST resin was monitored using an ultraviolet spectrometer with the wavelength set at 280 nm. The apparent mass of fractions corresponding to eluted protein was determined using SDS PAGE. The protein was eluted with 10mM glutathione. The appropriate fractions were collected and dialyzed out of the 10mM glutathione buffer and back into the original buffer. The protein was brought to a concentration of 2mg/ml and cleaved with a 1:100 ratio of HRV3C (GE Healthcare, Pittsburgh, PA) protease at 4°C for 24 hours. The protein was then run on a GST column again, the cleaved protein was in the flow through peak and the GST tag bound to the column and was eluted in later fractions with 10mM glutathione. The cleaved protein was dialyzed into gel filtration buffer with 5mM DTT. The protein was concentrated and brought down to a volume of approximately 6-8 mls and run on a size exclusion column (SEC) at one milliliter

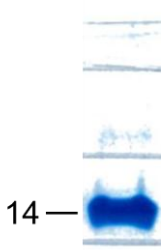

Figure 7. Purified MDM2 on SDS PAGE gel. The molecular weight is indicated on the left.

per minute flow rate. The fractions were run on an 18% SDS PAGE gel (figure 7) and the fractions containing the protein were dialyzed into 50mM sodium phosphate monobasic, 100mM sodium chloride, 1mM EDTA, 5mM DTT, and 0.02% sodium azide pH 7 and concentrated down to .3mM for NMR studies or dialyzed into 50mM sodium phosphate monobasic, 100mM sodium chloride, 1mM EDTA, 8mM βME, and 0.02% sodium azide pH 7 for ITC studies.

Nuclear Magnetic Resonance (NMR) Spectroscopy.

NMR spectroscopy is a technique that can be used to determine the structure of organic molecules with varying complexity. ^{1}H, ^{15}N, and ^{13}C are added to the media the *E. coli* are grown in effectively labeling the protein of interest with NMR active nuclei. NMR active nuclei contain an inherent magnetic moment that aligns with an applied magnetic field. In NMR spectroscopy the nuclei are perturbed by a radio frequency pulse. As they relax back to the original position and realign with the applied magnetic they emit a signal that is detected and referred to as resonance.

Using HSQC experiments to probe residue specific changes in the structure and dynamics of protein-protein interactions. An ^{1}H-^{15}N HSQC spectrum is collected to assess changes in protein structure by monitoring the nuclear magnetic resonance frequencies of the backbone amide and associated proton of an ^{15}N labeled protein. ^{1}H-^{15}N HSQC titration experiments were performed by labeling one protein and titrating in an unlabeled binding partner (figure 8). RPA70 was ^{15}N labeled in the HSQC titration experiments with

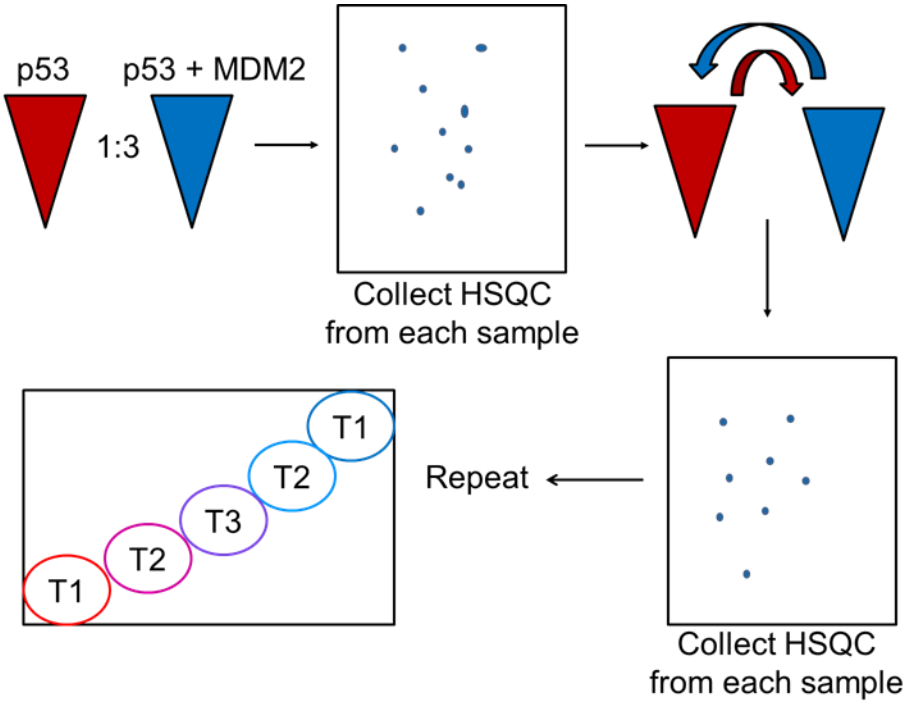

Figure 8. Cartoon schematic of ^{1}H-^{15}N HSQC NMR titration experiment. The red p53 sample contains only ^{15}N labeled p53. The blue sample contains the exact concentration of ^{15}N p53 plus a three molar excess of ^{14}N MDM2.

p53TAD. The MDM2 HSQC experiments contained ^{15}N labeled p53TAD. In the HSQC titration experiments two NMR samples were prepared. Both samples contained a ^{15}N-labeled protein at 100-300 μM. One of these samples also contained the unlabeled binding partner in a 2-3 fold stoichiometric excess. HSQC spectra were collected on both of these samples. Then an identical volume from each sample is removed and transferred to the other sample. Hamilton syringes were utilized to reduce sample loss during transfer and improve accuracy of the volume transferred. Two more HSQC spectra were collected after the transfer to assess changes in backbone structure and dynamics induced by the unlabeled protein binding partner. Volume transfers were made until both NMR samples contained the same concentration of the unlabeled protein-binding partner. The experiments were performed on a Varian VNMRS 600 MHz spectrometer equipped with a triple resonance pulse field Z-axis gradient cold probe. The sweep widths and complex points of the HSQC were 8012.8 (t_2) 62000 (t_1) Hz and 512 (t_2) 6128 (t_1), respectively (43). The experiments were performed at 25°C with uniformly labeled ^{15}N protein (p53TAD, RPA70Δ169, or RPA70Δ122) in 90%H_2O/10% D_2O, PBS buffer. Resonance assignments for human p53TAD and RPA70 were previously reported and the HSQC spectra peaks were inferred from these assignments (3, 74).

Paramagnetic Relaxation Enhancement (PRE). Paramagnetic Relaxation Enhancement is used to assess intramolecular distances in dynamic ensembles of intrinsically disordered proteins. This technique utilizes an unpaired electron from a (S-(2,2,5,5-tetramethyl-2,5-dihydro-1H-pyrrol-3-yl)methyl

methanesulfonothioate) (MTSL) paramagnetic group covalently attach to a cysteine to calculate intramolecular distances between 10-30 Å. Residues have increased relaxation rates when in close proximity to MTSL; which is seen on a NMR spectrum as peak broadening and decrease in peak intensity. Site directed mutagenesis, as previously described, was used to introduce a cysteine residue at position 28 in p53TAD. The E28C mutant sequence was confirmed (MWG, Operon). The p53Δ74_E28C protein was expressed and purified. Once purified and dialyzed into the NMR buffer with 4mM DTT three PD-10 columns (GE Healthcare, Pittsburgh, PA) were equilibrated with 25mls of NMR buffer (50mM sodium phosphate monobasic, 50mM sodium chloride, 1mM EDTA, and 0.02% sodium azide pH 6.8). Approximately, 2.5mls of 0.2mM p53Δ74_E28C was bound to an equilibrated PD-10 column. The protein was eluted with 3.5mls of buffer. The eluent was brought up to a total volume of 5mls. This was divided into 2.5mls and each was dialyzed again using the other two equilibrated PD-10 columns. The eluent dripped into a 15ml falcon tube with 100ul of MTSL suspended in ethanol. The eluent was pooled and was incubated at room temperature for one hour. 2.5mls was pulled off and was run through the PD-10 column again and then eluted with 3.5mls of NMR buffer. This was repeated every hour for three hours. At each hour time point 200µls was taken for mass spectrometry analysis. Direct injection ESI-mass spectrometry was performed to confirm that greater than 95% of the protein sample was MTSL labeled. After confirmation by mass spectroscopy, the ^{15}N labeled p53Δ74_E28C an HSQC

spectrum was collected. Afterwards, the MTSL group was reduced by the addition of ascorbic acid. Another HSQC was collected on the reduced sample.

NMR data analysis. Data analysis was performed using NMRview software on Linux OS. Raw data was collected as a .fid file and processed with a Perl script to convert it in to an .nv file that is readable by NMRview. Peak adjustments were made for most residues, excluding Prolines for RPA70Δ122, RPA70Δ169, p53Δ74_72P, p53Δ74_72R and p53Δ74_72P_E28C. The peak adjustments were correlated with each dataset. The datasets containing the amide nitrogen and proton chemical shifts, and peak intensities were converted to .txt files and imported into Microsoft Excel 2010. The total chemical shifts for the RPA70 were calculated using the formula, where H is equal to ^{1}H and N is equal to ^{15}N,

$$[\{H^2 + (N/5)^2\}/2]^{0.5}$$

The peak intensity values from the PRE experiments were calculated by dividing the peak intensities from the MTSL plus ascorbic acid HSQC by the peak intensity values from the MTSL HSQC spectrum.

Isothermal Titration Calorimetry.

ITC is a technique that measures the amount of heat that is released or absorbed when a protein and its ligand bind. This technique was employed to measure the binding stoichiometry (N), association constant (Ka), change in enthalpy (ΔH), and change in entropy (ΔS) between MDM2 (17-125) and p53TAD. The binding disassociation constant (Kd) can then be calculated. The

change in Gibbs energy (ΔG) can be calculated using the relationship ΔG= -RTlnKa = ΔH -TΔS, where R is the gas constant and T is the absolute temperature.

Protein purification was performed in parallel with MDM2 (17-125) and the p53TAD constructs, p53Δ74_K24N, p53Δ74_72R, p53Δ74_72P, p53Δ91_72R p53Δ91_72P. Each pair of proteins was co-dialyzed, with a 10,000+ fold dilution, into buffer (50mM sodium phosphate monobasic, 100mM sodium chloride, 1mM EDTA, 8mM βME, and 0.02% sodium azide pH 7). MDM2 was at 0.005mM in the cell and 0.05mM p53 was in the syringe and titrated in 7µl increments, with a total of 38 injections, and 300 seconds in between each titration point. Titrations were performed at 25°C and in triplicate. As a control, buffer was placed in the syringe and titrated into 0.005mM MDM2 to measure the heat of dilution. The raw ITC data was analyzed using Origin software.

Chapter 3: Results of the Interaction of RPA70 with p53

RPAΔ169 and Canine p53TAD ^{1}H-^{15}N HSQC Titration Experiment. RPA70 is highly conserved in mammals. The p53 protein sequence is less conserved (figure 9).

```
RPA70 Residues 1-122
Human       MVGQLSEGAIAAIMQKGDTNIKPILQVINIRPITTGNSPPRYRLLMSDGLNTLSSFMLAT 60
Canine      MVGHLSEGAIAAIMQQGETSIKPILQVINIRPITTGNSPPRYRLLMSDGLNTLSSFMLAT 60
            ***:***********:*:*.*********************************** ****
Human       QLNPLVEEEQLSSNCVCQIHRFIVNTLKDGRRVVILMELEVLKSAEAVGVKIGNPVPYNE GL 122
Canine      QLNPLVEEEQLSSNCICQINRFIVNTLKDGRRVVILMELNILKSAEAVGLKIGNPVPYNE GH 122
            **************:***:******************::********:********** *
p53 Transactivation Domain
Human       MEEPQSDPSVEPPLSQETFSDLWKLLPENNVLSPLPSQAMDDLMLSPDDIEQWFTEDPGP 60
Canine      MEESQSELNIDPPLSQETFSELWNLLPENNVLSSELCPAVDELLL-PESVVNWLDEDS-- 57
            ***.**: .::*********:**:*********. . *:*:*:* *:.: :*: **.
Human       DEAPRMP-EAAPRV------ 73
Canine      DDAPRMPATSAPTAPGPAPS 77
            *:***** :** .
```

Figure 9. The sequence alignment of human and canine RPA70 residues 1-122 and human and canine p53TAD. The p53 binding region of RPA70 is completely conserved in these homologues. The specific residues that undergo the largest chemical shifts in the presence of p53TAD are shown in red. The human p53TAD residues in the primary MDM2 binding site are shown in blue, and the human p53TAD residues important in binding RPA70 are shown in red.

It has been shown that there is a difference in the backbone dynamics for several p53TAD homologues (unpublished data from the Daughdrill lab); important for this experiment it has been shown that canine p53TAD is more dynamic that human p53TAD (43). The experiment was performed to assess if canine p53TAD would bind RPA70. Additionally, if complex formation occurred would the dynamic behavior have an effect on complex formation? Any difference in binding of RPA70 to human or canine p53TAD could be attributed to differences

in dynamics of the p53 transactivation domain, because of the high level of sequence conservation in the human and canine homologues of RPA70. Canine p53TAD was titrated into a ^{15}N labeled sample of RPA70Δ169. If canine p53TAD bound to RPA70Δ169 and showed reduced affinity for RPA70 it would indicate that the less dynamic human p53TAD aided in p53/RPA70 complex formation.

We found that canine p53TAD required a significantly higher concentration than human p53TAD to induce chemical shifts; indicating a lower affinity for

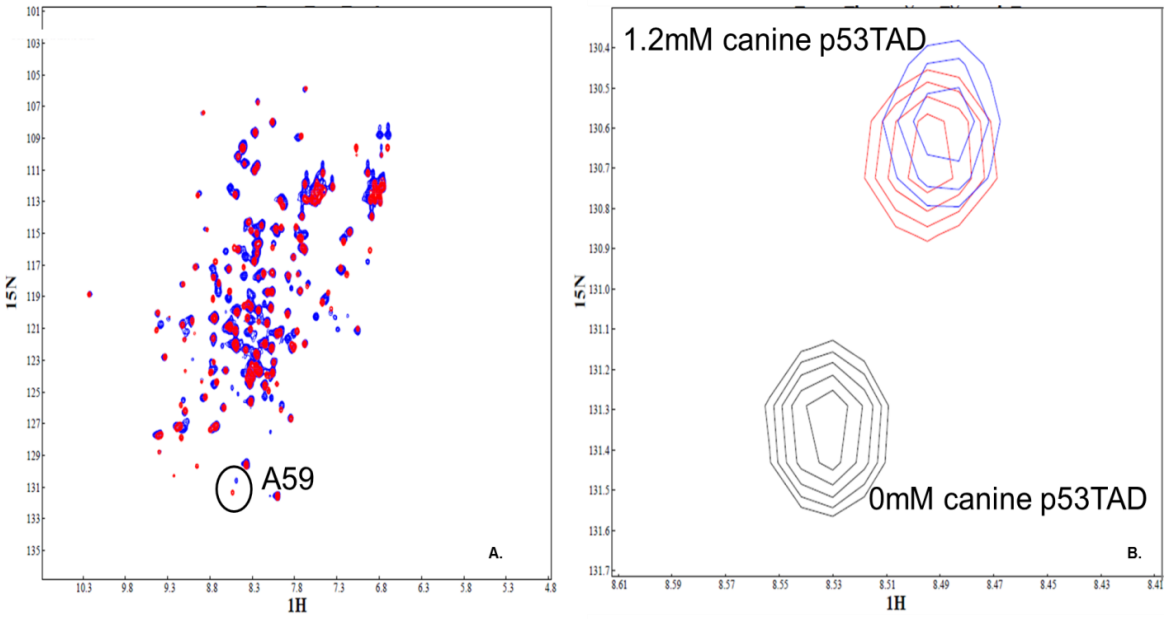

Figure 10. ^{1}H-^{15}N HSQC spectra of Canine p53TAD and RPAd169 titration experiment. A. An overlay of the first two spectra collected, red contains only RPA70Δ169 and blue contains RPA70Δ169 with a two molar excess of canine p53TAD. Alanine 59 is highlighted at the bottom of the spectra. B. A close up of Alanine 59 with the starting and ending concentration of Canine p53TAD.

RPA70Δ169. Figure 10 shows an overlay of the first two ^{1}H-^{15}N HSQC spectra. The red spectrum is the ^{15}N RPA70Δ169 sample and the blue spectrum is the ^{15}N RPA70Δ169 with a two-fold molar excess of ^{14}N canine p53TAD. The results indicate that canine p53TAD does form a complex with RPA70. The apparent

lower affinity of RPA70 and canine p53TAD suggests that the more dynamic canine p53TAD is influencing complex formation.

RPAΔ122 and Human p53TAD 1H-15N HSQC Titration Experiment. Previously, it was demonstrated that human p53TAD binds a basic cleft in DBDF of RPA70Δ169 (3). It has also been shown that single stranded DNA binds to the same basic cleft in DBDF; this suggests that a competitive mechanism may exist between ssDNA and p53TAD for RPA70 binding (3). We wanted to assess if the RPA70 flexible linker between DBDF and DBDA (figure 3) affected the binding interaction with human p53TAD. It is known that DBDF is important in protein-protein interactions and DBDA and DBDB have high affinity for single stranded

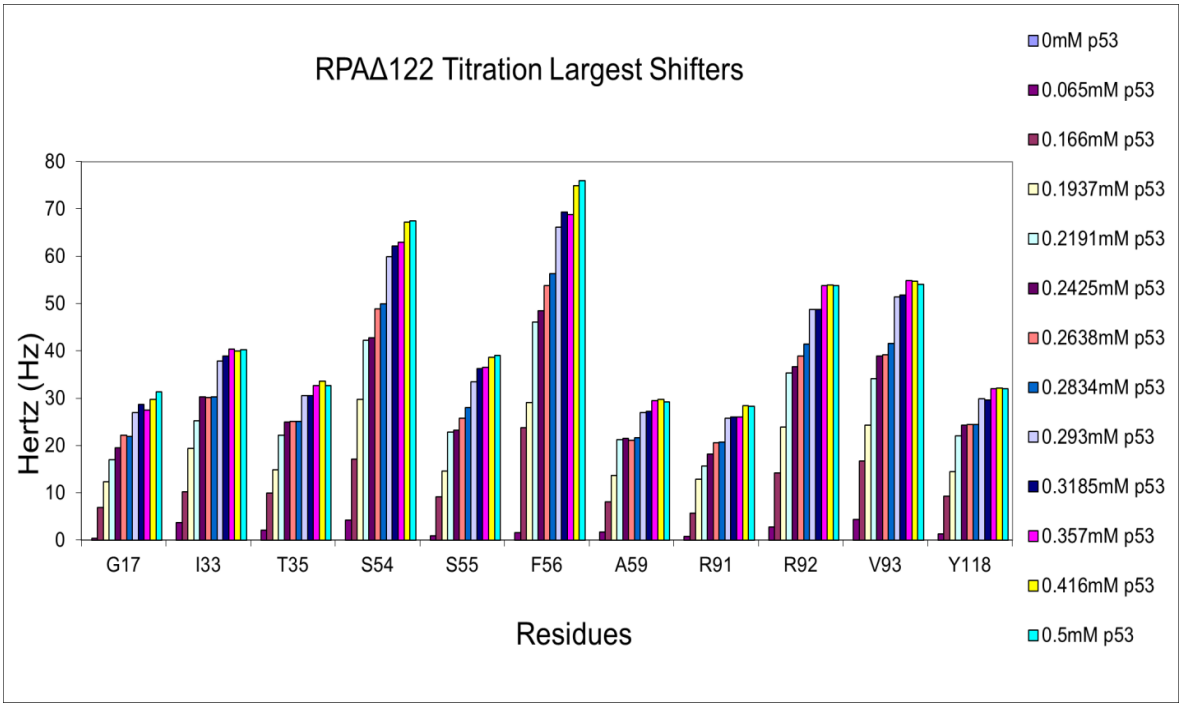

Figure 11. The chemical shift change in Hertz for the 11 residues on RPA70 that displayed the largest shift during p53TAD titration.

DNA. Investigating if the flexible linker affects complex formation between RPA70 and p53TAD would provide insight on how p53TAD may be involved in DNA damage response.

This titration was performed as previously described with ^{15}N labeled RPA70Δ122 and ^{14}N human p53TAD in a two-fold molar excess. The binding affinity and chemical shifts were similar in the RPAΔ169 and RPAΔ122 experiment with the largest shifts displayed by G17, I33, T35, S54, S55, F56, A59, R91, V93 and Y118 (figure 11). Each peak is representative of the ensemble average for that particular residue. The observed chemical shift changes occurred in small distinct increments. This is referred to as fast

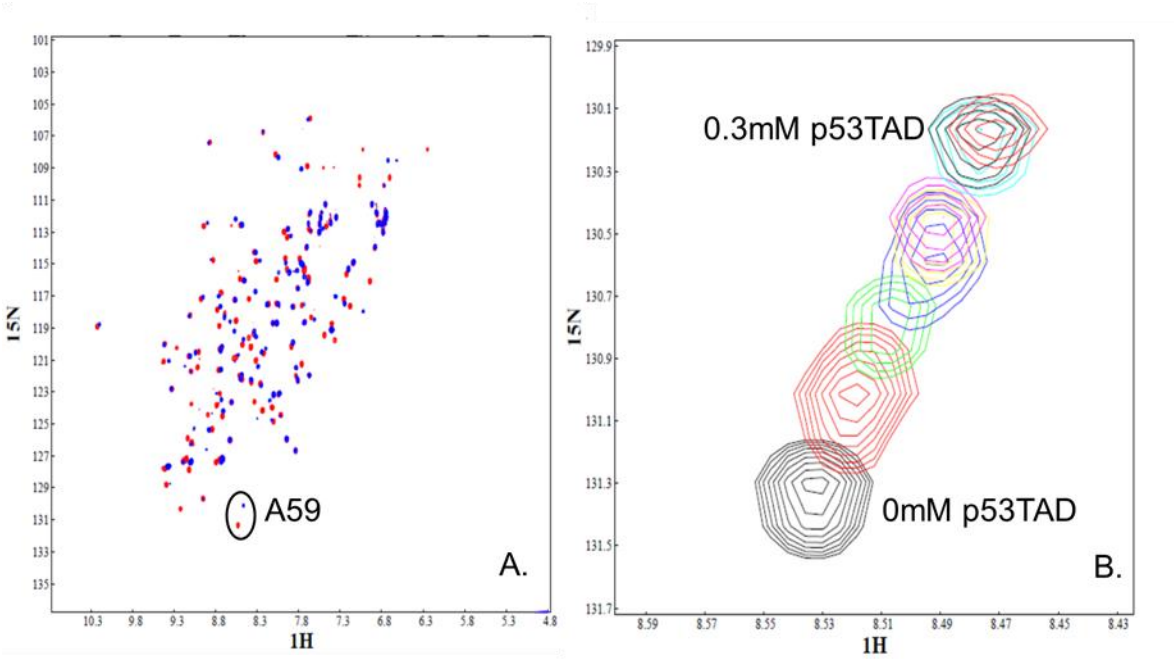

Figure 12. The ^{1}H-^{15}N HSQC spectra of the titration of ^{15}N RPAΔ122 and ^{14}N human p53TAD. A. An overlay of the first (red) and last (blue) titration points of RPAΔ122. The red spectrum does not contain any p53TAD and the blue spectrum contains 0.6mM p53TAD. B. The RPA70 residue Alanine 59 is shown at each titration point from 0.0mM to 0.3mM of p53TAD.

exchange; affirming that p53TAD and RPA70 have a low affinity (figure 12). The broadening of the resonances during the titration suggests the formation of multiple intermediates during the binding process. If the affinity was higher there would be two peaks observed; a free peak and a bound peak.

Based on these results we conclude that the flexible linker between DBDF and DBDA are not necessary for complex formation between RPA70 and p53TAD. The residues in RPA70 experience similar chemical shifts regardless of the presence of the flexible linker. RPA70Δ122 has low affinity for human p53TAD based on the peak behavior observed in this experiment.

Chapter 4: Results of the Interactions of MDM2 with p53

MDM2 and Human p53Δ74_72R ^{1}H-^{15}N HSQC Titration Experiment. In previous studies the binding of MDM2 and p53 was investigated primarily using short peptides of the p53 MDM2 binding site, typically encompassing residues 15-29 (75-83). Recently, it was shown that MDM2 binds to multiple distinct sites within the p53 transactivation domain, residues 18-26, 40-45, and 49-54 (73, 84). The primary MDM2 binding site includes residues 18-26, and the secondary binding site encompasses residues 40-55. We used the entire transactivation domain, residues 1-73 to assess binding to MDM2. Our approach was unique, not only for employing the entire transactivation domain, but because we used a higher ratio of MDM2 than had been previously reported. A similar study had been performed that did use a

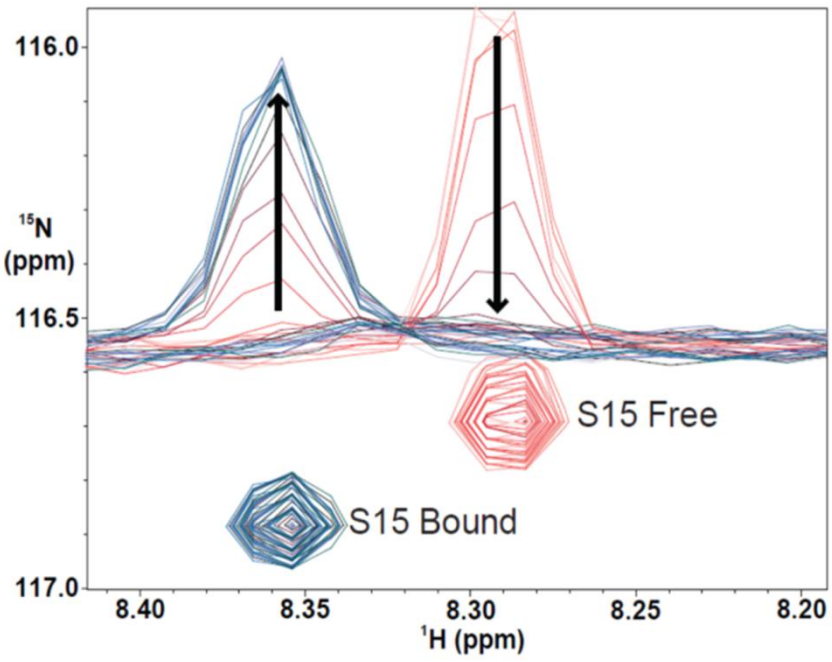

Figure 13 An overlay of 18 HSQC spectra of human p53 serine 15 when binding to MDM2. The one dimensional splice shows the peak intensity change during the titration. The free peak is shown in red and the bound peak is shown in blue.

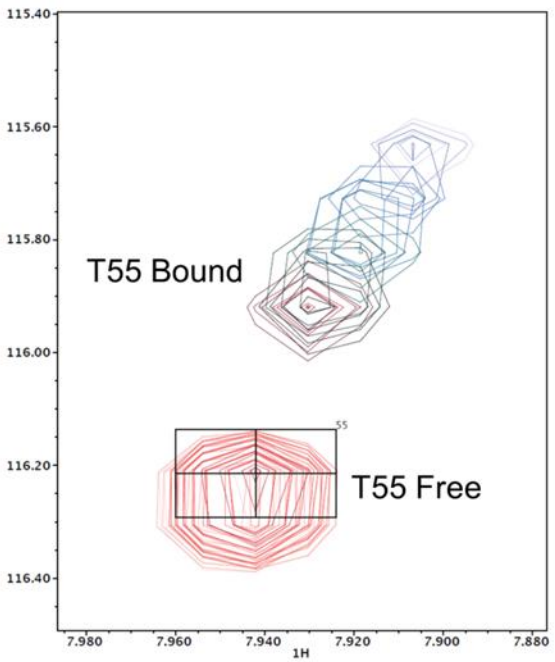

Figure 14 Threonine 55 peak behavior upon MDM2 titration. The free peak is shown in red and the bound peak is shown in blue.

longer p53TAD construct and HSQC titration, but the titration did not exceed a 1:2 ratio p53TAD to MDM2 (73).

We found that residues in the primary binding site, 15-29, behaved differently than the residues in the second site residues 40-55. In the primary binding site, the free peak disappeared and the bound peak appeared during the titration, consistent with a system in slow exchange that binds tightly (figure 13). There were only two peaks per residue in the primary binding site; a free peak and a bound peak. Binding in the primary binding site reached saturation at approximately a 1:1 ratio of p53TAD to MDM2. Bound peak intensity in the primary site reached a maximal value and remained constant once the primary site was saturated.

The 1:3 ratio we employed proved important for the peak behavior in the second site. Initially, the free peak disappeared and the bound peak appeared. However, once the primary site was saturated the bound peak displayed chemical shifts and peak intensity changes consistent with a system in fast exchange that binds weakly (figure 14). The peaks intensity changes were measured and plotted as a function of MDM2 concentration (figure 15). The

binding for the primary site is saturated at a stoichiometry of approximately 1:1, as shown by the intensity for the bound peak reaching a maximum. The peak intensity for the bound peak in the secondary site also reaches a maximum at a stoichiometry of 1:1 and then the bound peak loses intensity and experiences chemical shifts after additional MDM2 is added. This indicates that after the primary site is saturated, the apparent tight binding at the secondary site is actually weak (85, 86).

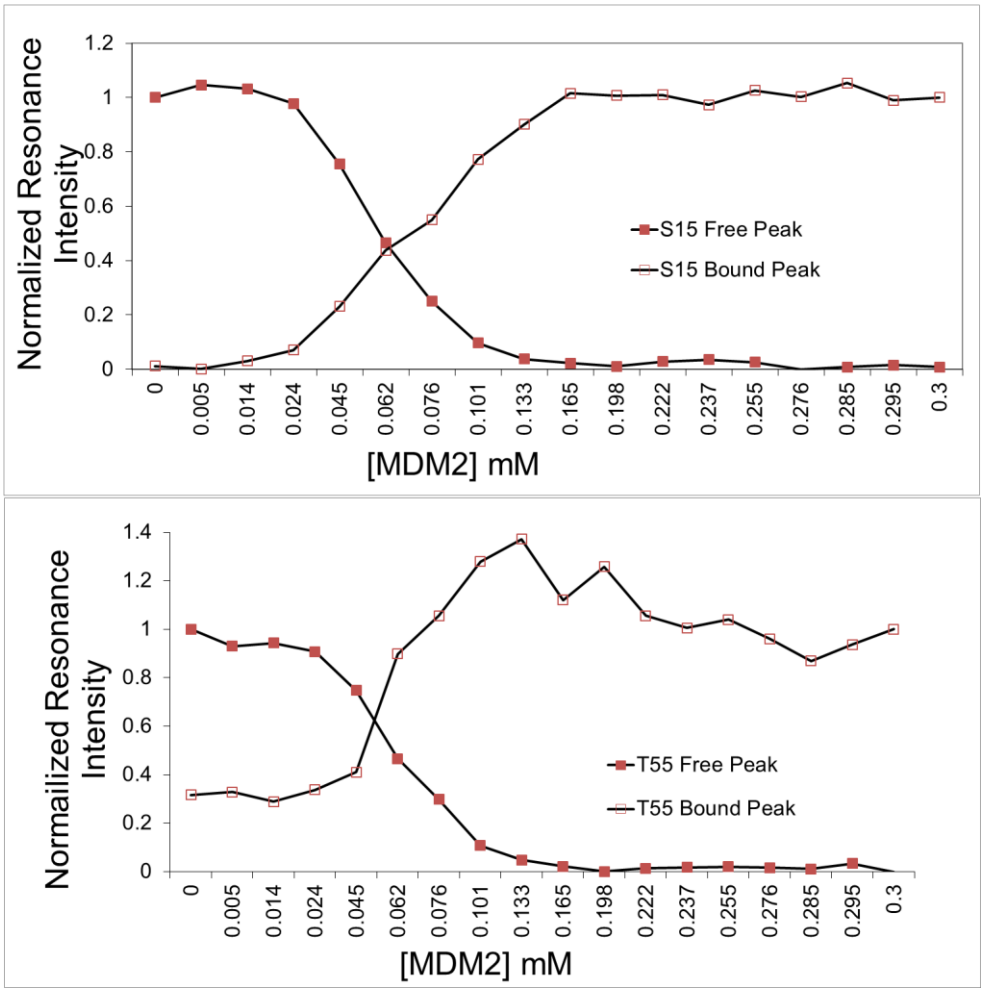

Figure 15. Peak intensity plotted as a function of MDM2 concentration. The primary site is depicted with Serine 15 and the secondary site is depicted with Threonine 55.

MDM2 and Human p53Δ74_72R_P27A ^{1}H-^{15}N HSQC Titration Experiment. It is known that prolines break alpha helices in structured proteins. The conserved proline at position 27 in p53TAD may be breaking the transient helix that forms in the primary MDM2 binding site. Site directed mutagenesis was used to create a protein ensemble that contained more helical propensity than the wild type p53TAD. This experiment was performed to assess how increasing the helical secondary structure of the primary binding influenced the affinity of MDM2 for p53TAD. p53TAD binds MDM2 in the form of an alpha helix; by introducing an alanine at position 27 p53TAD becomes more helical in

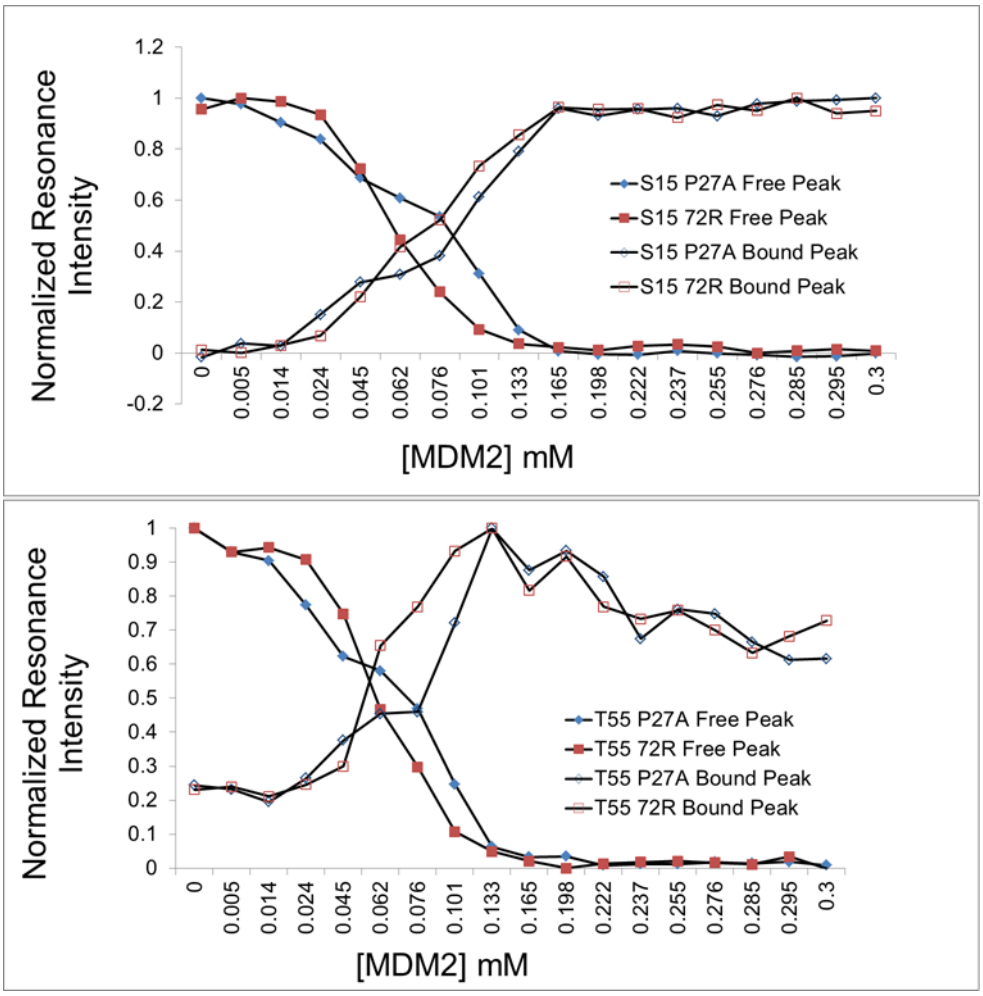

Figure 16. Serine 15 and Threonine 55 in p53TAD_P27A titration peak intensity plotted as a function of MDM2 concentration.

the MDM2 primary binding site. This experiment was designed to provide preliminary information about how coupled folding binding works in IDPs and how prolines affect transient secondary structure in these systems.

We found that the primary and secondary binding sites displayed similar behavior when compared to the p53Δ74_72R HSQC titration. However, the peak intensity falls more abruptly and in a linear fashion as compared to the p53 wild type in both binding sites. The peak intensity was plotted as a function of MDM2 concentration for both the primary and secondary MDM2 binding site (figure 16). The binding is saturated at the primary site in the P27A mutant at approximately the same concentration as the wild type. A reasonable explanation of the lower concentration of MDM2 needed to induce peak intensity decay and the linear relationship of the decay is the lower entropic barrier of binding the more helical p53 P27A to MDM2.

MDM2 and Human p53Δ74_K24N Isothermal Titration Calorimetry Experiment. The p53Δ74_K24N mutation was used to evaluate the lysine at position 24; a substitution to an asparagine was created by site directed mutagenesis. If the asparagine at residue 24 had higher binding affinity than the lysine wild type it would give credence to the hypothesis of lysine 24 forming a salt bridge that aided in stabilization of the transient helix present in the transactivation domains protein ensemble. The disassociation constant (Kd) and change in Gibbs free energy (ΔG) are listed for

Table 1. The ITC values of the point mutant K24N and p53TAD.

	p53Δ74_72R	p53Δ74_K24N
Kd	0.802666667	6.74E-08
ΔG	-8978.526667	-9.12E+03

the K24N mutant and wild type are shown in Table 1. The results indicate that the K24N point mutant has a lower disassociation constant and thus higher binding affinity for MDM2.

Chapter 5: Results of the Polymorphism at Position 72 in Human p53.

MDM2 and Human p53Δ74_72P ^{1}H-^{15}N HSQC Titration Experiment. Cellular studies have shown that the Arginine polymorphism at position 72 has a greater association with MDM2 compared to the Proline allele (5). A structural explanation of the biological differences has not been investigated until now. To investigate a structural basis for cellular function, we performed an NMR HSQC titration experiment with the proline allele to evaluate if there was a difference in chemical shifts or peak intensity as compared to our arginine allele data.

We titrated a ^{15}N labeled p53Δ74_72P sample with ^{14}N MDM2 and collected ^{1}H- ^{15}N HSQC spectra. Similar peak behavior in the primary and secondary site was observed in the proline allele as seen with the arginine allele. The primary site was saturated at stoichiometry of approximately 1:1 of p53TAD to MDM2. However, the peak intensity changes in both the primary and secondary site were different. The preliminary data suggests that a higher concentration of MDM2 might be required to cause the free peak intensity to decay in the proline allele (figure 17).

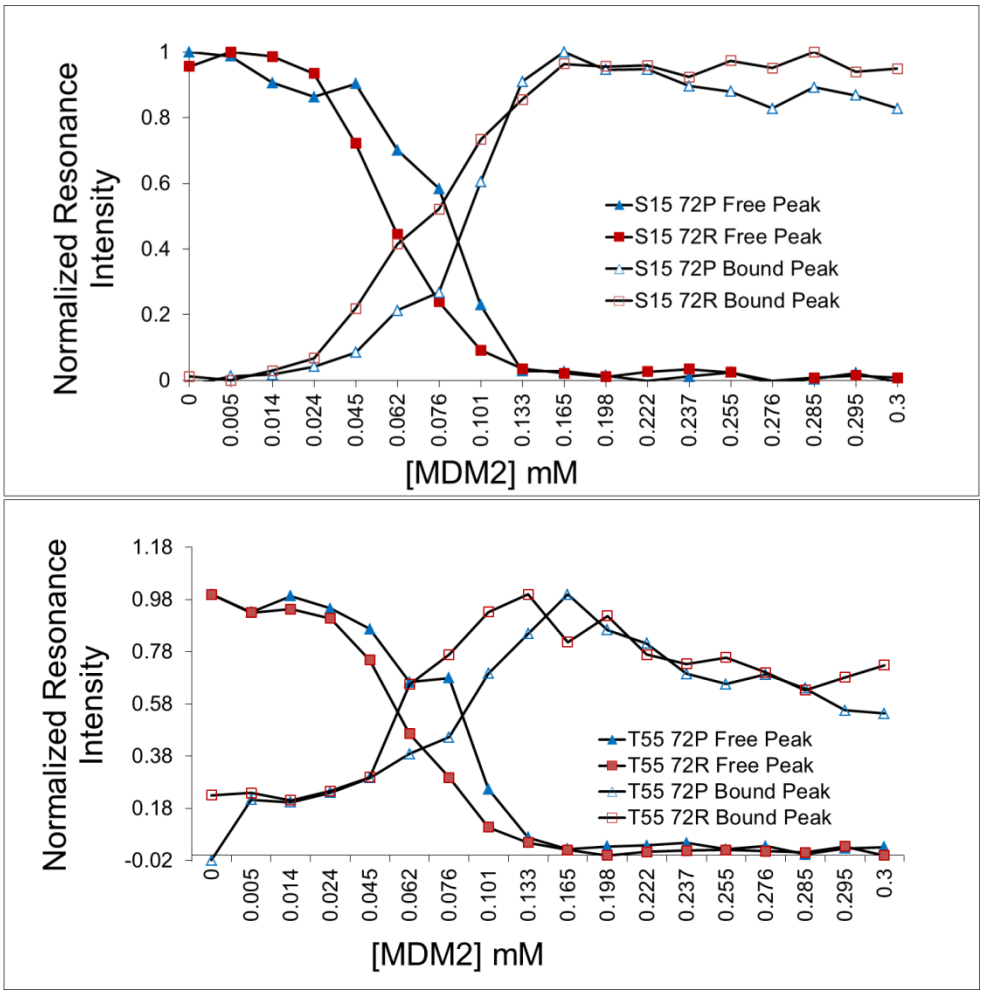

Figure 17. The polymorphism at position 72 titration experiments plotted with peak intensity as a function of MDM2.

MDM2 and Human p53TAD Isothermal Titration Calorimetry. As mentioned earlier, typically short peptides have been used to measure p53TAD binding to MDM2. We used varying lengths of p53TAD and to examine the thermodynamics of p53TAD and MDM2 complex formation. We used p53TAD constructs, Δ74_72R, Δ74_72P, Δ91_72R, and Δ91_72P. Both longer and shorter constructs were used to assess whether the single nucleotide polymorphism displayed different thermodynamics (Table 2). The long and short constructs of both alleles displayed similar values for ΔG and Kd.

Table 2. The ITC data collected comparing the single nucleotide polymorphism at position 72. The arginine polymorphism values are on the left and the proline values are on the right**.**

	p53Δ74_72R	p53Δ74_72P	p53Δ91_72R	p53Δ91_72P
Kd	3.45239E-07	1.71226E-07	1.6629E-07	2.64139E-07
ΔG	-8817.526667	-9235.4	-9044.06	-8978.526667

These data indicate that the biological difference may be due to a kinetic effect and not a thermodynamic effect.

Human p53Δ74_72R and p53Δ74_72P (1-73) Paramagnetic Relaxation Enhancement Experiment. This experiment was performed to compare the long-range interactions in the p53TAD polymorphism, p53Δ74_72R and p53 Δ74_72P. We know that MDM2 binds both the primary and secondary binding site. We know that the alleles display biological differences. However, it was not known how close the two binding sites are to each other in each allelic ensemble. The composition of conformations within the protein ensemble could be altered between alleles and be a potential explanation of the biological differences and differing affinity for MDM2.

The closer in proximity an individual residue is to the MTSL label the lower the resonance intensity quotient; this method gives reliable long-range distance estimates in intrinsically disordered proteins. The glutamic acid at position 28 was mutated to a cysteine so an MTSL label could be covalently attached adjacent to the primary MDM2 binding site and in between the primary and secondary sites. The resonance intensity quotients were measured and are plotted for the arginine and proline alleles in figure 18.

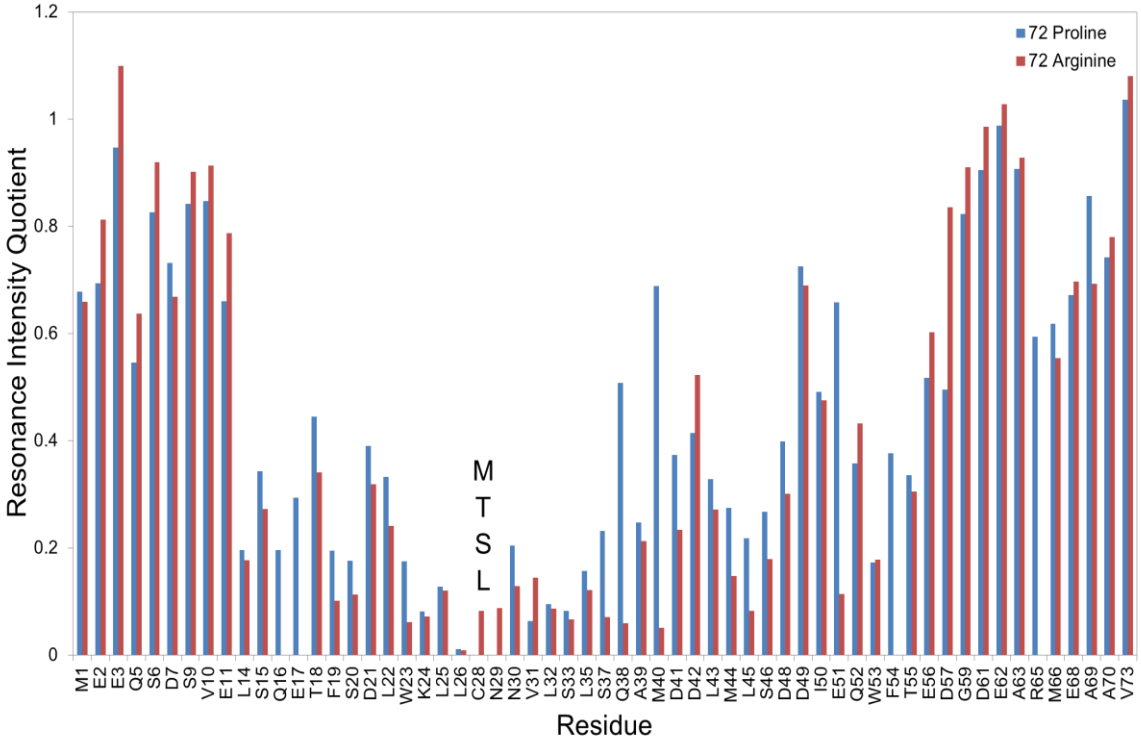

Figure 18. The long range interactions in the p53TAD polymorphism protein ensembles. The resonance intensity is shown on the X axis and the residue position is shown on the X axis. The proline allele is shown in blue and the arginine allele is shown in red.

The PRE data indicate that the primary and secondary binding sites are closer to each other in the arginine allele than they are in the proline allele. One potential explanation for the difference in proximity of the binding sites is that the proline allele has a more extended protein ensemble. If the proline allele had an extended ensemble it could lead to reduced affinity for MDM2. Furthermore, if the arginine allele had a collapsed ensemble with the two binding sites closer together it would cause a local concentration effect when MDM2 was present. This artificial increase in MDM2 availability between the two binding sites would be observed as the arginine allele having a higher affinity for MDM2; which has already been shown in cellular studies. Alternately, an electrostatic interaction could be influencing the closeness of the binding sites between the alleles. The

net charge of p53TAD is -13 or -14 depending on the allele, arginine and proline, respectively.

Another interesting observation is the low resonance intensity quotient at the carboxyl terminal around position 65 through 70 (figure 15). The MTSL label was attached to residue 28 and it is surprising to see residues interacting that far away. It is unexpected to find a long range interaction between residues spaced so far apart in an IDP due to the intrinsic nature of IDPs. The observation of long range interaction, such as the one shown here, provides clues to the behavior of IDPs and this knowledge could potentially lead to the structural explanation behind observed biological behavior.

Chapter 6: Discussion

RPA70. The RPA studies were performed to assess the evolution of intrinsic disorder in the p53 transactivation domain by investigating the human and canine p53TAD/RPA complex. We demonstrated that canine p53TAD does bind to RPA70Δ169. This experiment showed that a homologue of p53TAD that has varying dynamics within its protein ensemble binds RPA70. Despite the evolutionary conservation of the RPA70/p53TAD interaction complex formation variations are seen between the canine and human NMR spectra. The canine p53TAD had a lower apparent affinity than the human p53TAD. It took 1:4 molar ratio of canine p53 to induce the chemical shifts seen with a 1:2 molar ratio of human p53TAD. Furthermore, the less dynamic human p53TAD binds RPA70 with higher affinity. This data suggests that the dynamic behavior of intrinsically disordered proteins may impact their biological function.

We also examined the intrinsically disordered linker (IDL) in RPA between DBDF and DBDA to evaluate if the intrinsically disordered linker played a role in complex formation with p53TAD. We showed that the flexible linker between DBDF and DBDA in RPA70 does not have a large impact on complex formation with the p53 transactivation domain. The residues involved with binding p53TAD displayed similar chemical shifts and peak intensity in the presence and absence of the disordered linker domain. The largest chemical shifts were seen for residues G17, I33, T35, S54, S55, F56, A59, R91, V93 and Y118. These results

align very well with published chemical shifts for RPAΔ169 induced by human p53TAD binding (3). The flexible linker between DBDF and DBDA may have evolved as a mechanism to aid in response to DNA damage. The linker tethers two domains together; the first having affinity for p53 and the second having high affinity for single stranded DNA. RPA70 could bind to p53 blocking the MDM2/p53 interaction. If the cell experienced stress and DNA damage, RPA could then release p53 and bind single stranded DNA. The p53 protein could then be activated and would go on to induce growth arrest, DNA repair, or apoptosis.

MDM2. The HSQC NMR experiments showed that the peaks in the primary binding site behaved differently than the peaks in the secondary binding site. In the primary binding site, the free peak would disappear and the bound peak would appear and this was associated with marked changes in peak intensity. The second binding site displayed chemical shifts and peak intensities decreased as more MDM2 was added. The apparent high affinity, as indicated by slow exchange, in the second binding site could be caused by high local concentration of MDM2 that would be present at concentrations below saturation (figure 19). Once the first site is saturated this effect is alleviated and the true lower affinity becomes apparent.

The ^{1}H-^{15}N HSQC titration with the P27A point mutant and MDM2 showed that binding saturation occurred at roughly the same concentration as the wild type. However, it took a smaller amount of MDM2 to induce a decrease in peak intensity compared to wild type p53TAD. The free peak intensity decay is linear

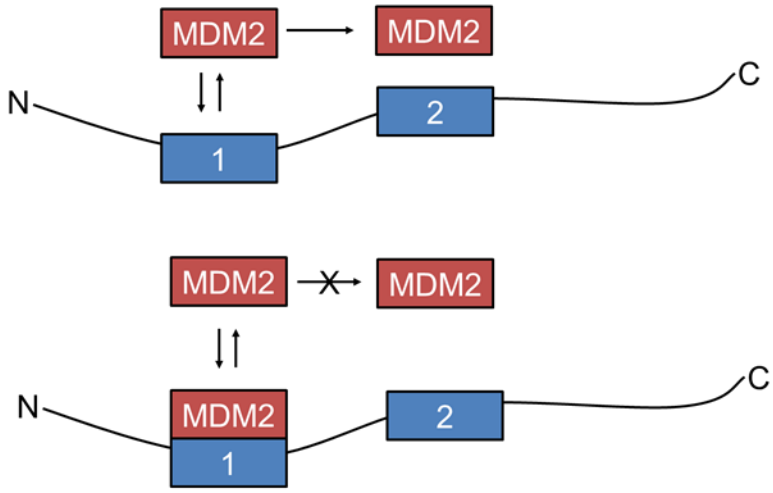

Figure 19. A schematic of the local concentration effect of MDM2 on the second binding site in p53TAD. The primary and secondary MDM2 binding sites are shown in blue and MDM2 is depicted in red. The top schematic depicts unsaturated p53TAD and the lower schematic represents saturation of MDM2 in the primary binding site.

when plotted as a function of MDM2 concentration. One possible explanation is that the more helical P27A is experiencing conformational selection when binding MDM2. The less helical wild type requires a higher concentration of MDM2 to induce the free peak intensity decrease and does not have a linear decay. The wild type may be following a form of coupled folding-binding referred to as induced fit. In the induced fit mode of binding there are nonspecific interactions that lead to a conformational change and then tighter binding occurs.

Polymorphism at Position 72. These p53TAD and MDM2 studies were performed to investigate the effects of the single nucleotide polymorphism at position 72 in p53TAD and to assess the thermodynamics of complex formation between p53TAD and MDM2. When we compared the results from the PRE experiments for the polymorphism we found a difference in the proximity of the first and second binding sites. In the arginine allele, the binding sites were closer to each other than they were in the proline allele. One potential explanation is

that the proline allele has a more extended protein ensemble and the arginine allele has a more collapsed protein ensemble (figure 20). This might be expected based on the presence of the extra positive charge in a protein that has a net negative charge of -13. However, it is important to note that this polymorphism occurs at the second to last residue used in the constructs, which may influence the results. A longer construct should be used to verify these results.

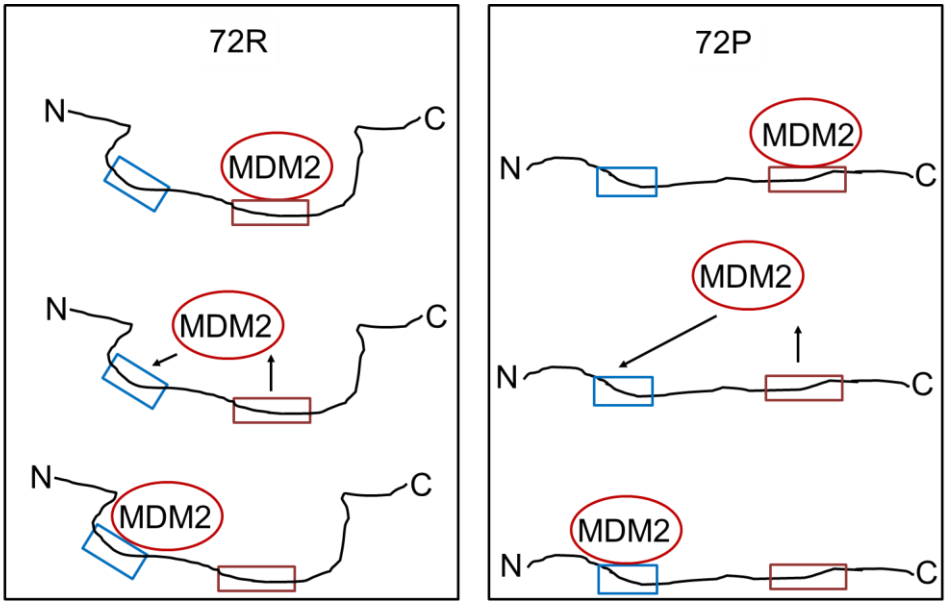

72R collapsed ensemble→ local concentration effect → higher affinity
72P elongated ensemble →further distance between sites → lower affinity

Figure 20. A schematic of the possible compositions of the protein ensembles of the arginine and proline alleles. The arginine allele is more collapsed causing a higher local concentration effect of MDM2 than what is seen in the proline protein ensemble.

Based on the PRE data and the NMR titration results, it would be reasonable to expect that the ITC data would show that the arginine allele would have a higher affinity for MDM2 than the proline allele. However, short and long constructs of each SNP were employed and there was not a significant difference in the

binding disassociation constants (Kd). The full length arginine has been shown to have higher affinity for MDM2 than the proline allele in cellular studies (5). Additionally, long range interactions have been shown in the intrinsically disordered p53 transactivation domain (4, 87). It is clear that more experimentation needs to be done to understand how the complex formation occurs in respect to the single nucleotide polymorphism at position 72 in p53TAD.

Future directions for this project would include PRE experiments on the longer polymorphism constructs to determine in the distance between the binding sites is similar to those calculated for the shorter constructs. Relaxation dispersion NMR experiments could be employed to investigate the kinetic differences between the alleles; potentially explaining the similarity in thermodynamics from the ITC data. Before this work began a structural explanation of the biological differences displayed by polymorphism was lacking. This work has provided preliminary clues about the mechanism of this system. It has been shown that there is a correlation with latitude and the distribution of the proline and arginine allele. It is also known that populations are more susceptible to certain cancers and have different cancer outcomes. It would be interesting to investigate the evolutionary implications of this allele, and how it may have played a role in designating p53, in the words of Levine “The Guardian of the Genome”.

References Cited

1. Vogelstein B, Lane D, Levine AJ. Surfing the p53 network. Nature. 2000;408(6810):307-10. Epub 2000/12/01. doi: 10.1038/35042675. PubMed PMID: 11099028.

2. Selivanova G, Wiman KG. p53: a cell cycle regulator activated by DNA damage. Advances in cancer research. 1995;66:143-80. Epub 1995/01/01. PubMed PMID: 7793313.

3. Vise PD, Baral B, Latos AJ, Daughdrill GW. NMR chemical shift and relaxation measurements provide evidence for the coupled folding and binding of the p53 transactivation domain. Nucleic acids research. 2005;33(7):2061-77. Epub 2005/04/13. doi: 10.1093/nar/gki336. PubMed PMID: 15824059; PubMed Central PMCID: PMC1075921.

4. Vise P, Baral B, Stancik A, Lowry DF, Daughdrill GW. Identifying long-range structure in the intrinsically unstructured transactivation domain of p53. Proteins. 2007;67(3):526-30. Epub 2007/03/06. doi: 10.1002/prot.21364. PubMed PMID: 17335006.

5. Dumont P, Leu JI, Della Pietra AC, 3rd, George DL, Murphy M. The codon 72 polymorphic variants of p53 have markedly different apoptotic potential. Nature genetics. 2003;33(3):357-65. Epub 2003/02/05. doi: 10.1038/ng1093. PubMed PMID: 12567188.

6. Soussi T. The history of p53. A perfect example of the drawbacks of scientific paradigms. EMBO reports. 2010;11(11):822-6. Epub 2010/10/12. doi: 10.1038/embor.2010.159. PubMed PMID: 20930848; PubMed Central PMCID: PMC2966958.

7. Chang C, Simmons DT, Martin MA, Mora PT. Identification and partial characterization of new antigens from simian virus 40-transformed mouse cells. Journal of virology. 1979;31(2):463-71. Epub 1979/08/01. PubMed PMID: 225565; PubMed Central PMCID: PMC353469.

8. Kress M, May E, Cassingena R, May P. Simian virus 40-transformed cells express new species of proteins precipitable by anti-simian virus 40 tumor serum. Journal of virology. 1979;31(2):472-83. Epub 1979/08/01. PubMed PMID: 225566; PubMed Central PMCID: PMC353470.

9. Rotter V, Witte ON, Coffman R, Baltimore D. Abelson murine leukemia virus-induced tumors elicit antibodies against a host cell protein, P50. Journal of virology. 1980;36(2):547-55. Epub 1980/11/01. PubMed PMID: 6159484; PubMed Central PMCID: PMC353673.

10. DeLeo AB, Jay G, Appella E, Dubois GC, Law LW, Old LJ. Detection of a transformation-related antigen in chemically induced sarcomas and other transformed cells of the mouse. Proceedings of the National Academy of Sciences of the United States of America. 1979;76(5):2420-4. Epub 1979/05/01. PubMed PMID: 221923; PubMed Central PMCID: PMC383613.

11. Lane DP, Crawford LV. T antigen is bound to a host protein in SV40-transformed cells. Nature. 1979;278(5701):261-3. Epub 1979/03/15. PubMed PMID: 218111.

12. Linzer DI, Maltzman W, Levine AJ. The SV40 A gene product is required for the production of a 54,000 MW cellular tumor antigen. Virology. 1979;98(2):308-18. Epub 1979/10/30. PubMed PMID: 228475.

13. Leppard K, Crawford L. Monoclonal antibodies displaying a novel species specificity for the primate transformation-related protein, p53. The EMBO journal. 1983;2(9):1457-64. Epub 1983/01/01. PubMed PMID: 11892796; PubMed Central PMCID: PMC555307.

14. Reich NC, Levine AJ. Growth regulation of a cellular tumour antigen, p53, in nontransformed cells. Nature. 1984;308(5955):199-201. Epub 1984/03/08. PubMed PMID: 6366574.

15. Milner J, McCormick F. Lymphocyte stimulation: concanavalin A induces the expression of a 53K protein. Cell biology international reports. 1980;4(7):663-7. Epub 1980/07/01. PubMed PMID: 7397796.

16. Mercer WE, Nelson D, DeLeo AB, Old LJ, Baserga R. Microinjection of monoclonal antibody to protein p53 inhibits serum-induced DNA synthesis in 3T3 cells. Proceedings of the National Academy of Sciences of the United States of America. 1982;79(20):6309-12. Epub 1982/10/01. PubMed PMID: 6292898; PubMed Central PMCID: PMC347110.

17. Mercer WE, Avignolo C, Baserga R. Role of the p53 protein in cell proliferation as studied by microinjection of monoclonal antibodies. Molecular and cellular biology. 1984;4(2):276-81. Epub 1984/02/01. PubMed PMID: 6366518; PubMed Central PMCID: PMC368692.

18. Calabretta B, Kaczmarek L, Selleri L, Torelli G, Ming PM, Ming SC, et al. Growth-dependent expression of human Mr 53,000 tumor antigen messenger RNA in normal and neoplastic cells. Cancer research. 1986;46(11):5738-42. Epub 1986/11/01. PubMed PMID: 3019534.

19. Shohat O, Greenberg M, Reisman D, Oren M, Rotter V. Inhibition of cell growth mediated by plasmids encoding p53 anti-sense. Oncogene. 1987;1(3):277-83. Epub 1987/01/01. PubMed PMID: 2455263.

20. Eliyahu D, Raz A, Gruss P, Givol D, Oren M. Participation of p53 cellular tumour antigen in transformation of normal embryonic cells. Nature. 1984;312(5995):646-9. Epub 1984/12/13. PubMed PMID: 6095116.

21. Parada LF, Land H, Weinberg RA, Wolf D, Rotter V. Cooperation between gene encoding p53 tumour antigen and ras in cellular transformation. Nature. 1984;312(5995):649-51. Epub 1984/12/13. PubMed PMID: 6390217.

22. Jenkins JR, Rudge K, Currie GA. Cellular immortalization by a cDNA clone encoding the transformation-associated phosphoprotein p53. Nature. 1984;312(5995):651-4. Epub 1984/12/13. PubMed PMID: 6095117.

23. Jenkins JR, Rudge K, Chumakov P, Currie GA. The cellular oncogene p53 can be activated by mutagenesis. Nature. 1985;317(6040):816-8. Epub 1985/10/06. PubMed PMID: 3903515.

24. Mowat M, Cheng A, Kimura N, Bernstein A, Benchimol S. Rearrangements of the cellular p53 gene in erythroleukaemic cells transformed by Friend virus. Nature. 1985;314(6012):633-6. Epub 1985/04/18. PubMed PMID: 3990796.

25. Malkin D, Li FP, Strong LC, Fraumeni JF, Jr., Nelson CE, Kim DH, et al. Germ line p53 mutations in a familial syndrome of breast cancer, sarcomas, and other neoplasms. Science. 1990;250(4985):1233-8. Epub 1990/12/10. PubMed PMID: 1978757.

26. Srivastava S, Zou ZQ, Pirollo K, Blattner W, Chang EH. Germ-line transmission of a mutated p53 gene in a cancer-prone family with Li-Fraumeni syndrome. Nature. 1990;348(6303):747-9. Epub 1990/12/20. doi: 10.1038/348747a0. PubMed PMID: 2259385.

27. Finlay CA, Hinds PW, Levine AJ. The p53 proto-oncogene can act as a suppressor of transformation. Cell. 1989;57(7):1083-93. Epub 1989/06/30. PubMed PMID: 2525423.

28. Hinds P, Finlay C, Levine AJ. Mutation is required to activate the p53 gene for cooperation with the ras oncogene and transformation. Journal of virology. 1989;63(2):739-46. Epub 1989/02/01. PubMed PMID: 2642977; PubMed Central PMCID: PMC247745.

29. Baker SJ, Fearon ER, Nigro JM, Hamilton SR, Preisinger AC, Jessup JM, et al. Chromosome 17 deletions and p53 gene mutations in colorectal carcinomas. Science. 1989;244(4901):217-21. Epub 1989/04/14. PubMed PMID: 2649981.

30. Takahashi T, Nau MM, Chiba I, Birrer MJ, Rosenberg RK, Vinocour M, et al. p53: a frequent target for genetic abnormalities in lung cancer. Science. 1989;246(4929):491-4. Epub 1989/10/27. PubMed PMID: 2554494.

31. Essmann F, Schulze-Osthoff K. Translational approaches targeting the p53 pathway for anticancer therapy. British journal of pharmacology. 2011. Epub 2011/07/02. doi: 10.1111/j.1476-5381.2011.01570.x. PubMed PMID: 21718309.

32. Harris SL, Levine AJ. The p53 pathway: positive and negative feedback loops. Oncogene. 2005;24(17):2899-908. Epub 2005/04/20. doi: 10.1038/sj.onc.1208615. PubMed PMID: 15838523.

33. Levine AJ. p53, the cellular gatekeeper for growth and division. Cell. 1997;88(3):323-31. Epub 1997/02/07. PubMed PMID: 9039259.

34. Burns TF, El-Deiry WS. The p53 pathway and apoptosis. Journal of cellular physiology. 1999;181(2):231-9. Epub 1999/09/25. doi: 10.1002/(SICI)1097-4652(199911)181:2<231::AID-JCP5>3.0.CO;2-L. PubMed PMID: 10497302.

35. Vousden KH. Apoptosis. p53 and PUMA: a deadly duo. Science. 2005;309(5741):1685-6. Epub 2005/09/10. doi: 10.1126/science.1118232. PubMed PMID: 16151000.

36. Vogelstein B, Kinzler KW. Tumour-suppressor genes. X-rays strike p53 again. Nature. 1994;370(6486):174-5. Epub 1994/07/21. doi: 10.1038/370174a0. PubMed PMID: 8028656.

37. Wright PE, Dyson HJ. Intrinsically unstructured proteins: re-assessing the protein structure-function paradigm. Journal of molecular biology. 1999;293(2):321-31. Epub 1999/11/05. doi: 10.1006/jmbi.1999.3110. PubMed PMID: 10550212.

38. Dyson HJ, Wright PE. Insights into the structure and dynamics of unfolded proteins from nuclear magnetic resonance. Adv Protein Chem. 2002;62:311-40. Epub 2002/11/07. PubMed PMID: 12418108.

39. Uversky VN. What does it mean to be natively unfolded? European journal of biochemistry / FEBS. 2002;269(1):2-12. Epub 2002/01/11. PubMed PMID: 11784292.

40. Iakoucheva LM, Brown CJ, Lawson JD, Obradovic Z, Dunker AK. Intrinsic disorder in cell-signaling and cancer-associated proteins. Journal of molecular biology. 2002;323(3):573-84. Epub 2002/10/17. PubMed PMID: 12381310.

41. Dosztanyi Z, Csizmok V, Tompa P, Simon I. The pairwise energy content estimated from amino acid composition discriminates between folded and intrinsically unstructured proteins. Journal of molecular biology. 2005;347(4):827-39. Epub 2005/03/17. doi: 10.1016/j.jmb.2005.01.071. PubMed PMID: 15769473.

42. Olson KE, Narayanaswami P, Vise PD, Lowry DF, Wold MS, Daughdrill GW. Secondary structure and dynamics of an intrinsically unstructured linker domain. Journal of biomolecular structure & dynamics. 2005;23(2):113-24. Epub 2005/08/03. PubMed PMID: 16060685.

43. Daughdrill GW, Borcherds WM, Wu H. Disorder predictors also predict backbone dynamics for a family of disordered proteins. PloS one. 2011;6(12):e29207. Epub 2011/12/24. doi: 10.1371/journal.pone.0029207. PubMed PMID: 22195023; PubMed Central PMCID: PMC3240651.

44. Uversky VN. Natively unfolded proteins: a point where biology waits for physics. Protein science : a publication of the Protein Society. 2002;11(4):739-56. Epub 2002/03/23. doi: 10.1110/ps.4210102. PubMed PMID: 11910019; PubMed Central PMCID: PMC2373528.

45. Cheng Y, LeGall T, Oldfield CJ, Mueller JP, Van YY, Romero P, et al. Rational drug design via intrinsically disordered protein. Trends Biotechnol. 2006;24(10):435-42. Epub 2006/08/01. doi: S0167-7799(06)00184-3 [pii]

10.1016/j.tibtech.2006.07.005. PubMed PMID: 16876893.

46. Dyson HJ, Wright PE. Coupling of folding and binding for unstructured proteins. Curr Opin Struct Biol. 2002;12(1):54-60. Epub 2002/02/13. doi: S0959440X02002890 [pii]. PubMed PMID: 11839490.

47. Dyson HJ, Wright PE. Intrinsically unstructured proteins and their functions. Nat Rev Mol Cell Biol. 2005;6(3):197-208. Epub 2005/03/02. doi: nrm1589 [pii]

10.1038/nrm1589. PubMed PMID: 15738986.

48. Daughdrill GW, Narayanaswami P, Gilmore SH, Belczyk A, Brown CJ. Dynamic behavior of an intrinsically unstructured linker domain is conserved in the face of negligible amino acid sequence conservation. Journal of molecular evolution. 2007;65(3):277-88. Epub 2007/08/28. doi: 10.1007/s00239-007-9011-2. PubMed PMID: 17721672.

49. Plaxco KW, Gross M. Cell biology. The importance of being unfolded. Nature. 1997;386(6626):657, 9. Epub 1997/04/17. doi: 10.1038/386657a0. PubMed PMID: 9109481.

50. Demchenko AP. Recognition between flexible protein molecules: induced and assisted folding. J Mol Recognit. 2001;14(1):42-61. Epub 2001/02/17. doi: 10.1002/1099-1352(200101/02)14:1<42::AID-JMR518>3.0.CO;2-8 [pii]

10.1002/1099-1352(200101/02)14:1<42::AID-JMR518>3.0.CO;2-8. PubMed PMID: 11180561.

51. Bell S, Klein C, Muller L, Hansen S, Buchner J. p53 contains large unstructured regions in its native state. Journal of molecular biology. 2002;322(5):917-27. Epub 2002/10/09. PubMed PMID: 12367518.

52. Cho Y, Gorina S, Jeffrey PD, Pavletich NP. Crystal structure of a p53 tumor suppressor-DNA complex: understanding tumorigenic mutations. Science. 1994;265(5170):346-55. Epub 1994/07/15. PubMed PMID: 8023157.

53. Gottlieb TM, Oren M. p53 in growth control and neoplasia. Biochimica et biophysica acta. 1996;1287(2-3):77-102. Epub 1996/06/07. PubMed PMID: 8672531.

54. Iftode C, Daniely Y, Borowiec JA. Replication protein A (RPA): the eukaryotic SSB. Critical reviews in biochemistry and molecular biology. 1999;34(3):141-80. Epub 1999/09/03. doi: 10.1080/10409239991209255. PubMed PMID: 10473346.

55. Wold MS, Kelly T. Purification and characterization of replication protein A, a cellular protein required for in vitro replication of simian virus 40 DNA. Proceedings of the National Academy of Sciences of the United States of

America. 1988;85(8):2523-7. Epub 1988/04/01. PubMed PMID: 2833742; PubMed Central PMCID: PMC280029.

56. Erdile LF, Heyer WD, Kolodner R, Kelly TJ. Characterization of a cDNA encoding the 70-kDa single-stranded DNA-binding subunit of human replication protein A and the role of the protein in DNA replication. The Journal of biological chemistry. 1991;266(18):12090-8. Epub 1991/06/25. PubMed PMID: 2050703.

57. Abramova NA, Russell J, Botchan M, Li R. Interaction between replication protein A and p53 is disrupted after UV damage in a DNA repair-dependent manner. Proceedings of the National Academy of Sciences of the United States of America. 1997;94(14):7186-91. Epub 1997/07/08. PubMed PMID: 9207066; PubMed Central PMCID: PMC23787.

58. Dutta A, Ruppert JM, Aster JC, Winchester E. Inhibition of DNA replication factor RPA by p53. Nature. 1993;365(6441):79-82. Epub 1993/09/02. doi: 10.1038/365079a0. PubMed PMID: 8361542.

59. Li R, Botchan MR. The acidic transcriptional activation domains of VP16 and p53 bind the cellular replication protein A and stimulate in vitro BPV-1 DNA replication. Cell. 1993;73(6):1207-21. Epub 1993/06/18. PubMed PMID: 8390328.

60. Miller SD, Moses K, Jayaraman L, Prives C. Complex formation between p53 and replication protein A inhibits the sequence-specific DNA binding of p53 and is regulated by single-stranded DNA. Molecular and cellular biology. 1997;17(4):2194-201. Epub 1997/04/01. PubMed PMID: 9121469; PubMed Central PMCID: PMC232068.

61. Oliner JD, Kinzler KW, Meltzer PS, George DL, Vogelstein B. Amplification of a gene encoding a p53-associated protein in human sarcomas. Nature. 1992;358(6381):80-3. Epub 1992/07/02. doi: 10.1038/358080a0. PubMed PMID: 1614537.

62. Momand J, Zambetti GP, Olson DC, George D, Levine AJ. The mdm-2 oncogene product forms a complex with the p53 protein and inhibits p53-mediated transactivation. Cell. 1992;69(7):1237-45. Epub 1992/06/26. PubMed PMID: 1535557.

63. Barak Y, Oren M. Enhanced binding of a 95 kDa protein to p53 in cells undergoing p53-mediated growth arrest. The EMBO journal. 1992;11(6):2115-21. Epub 1992/06/01. PubMed PMID: 1600943; PubMed Central PMCID: PMC556678.

64. Ara S, Lee PS, Hansen MF, Saya H. Codon 72 polymorphism of the TP53 gene. Nucleic acids research. 1990;18(16):4961. Epub 1990/08/25. PubMed PMID: 1975675; PubMed Central PMCID: PMC332028.

65. Thomas M, Kalita A, Labrecque S, Pim D, Banks L, Matlashewski G. Two polymorphic variants of wild-type p53 differ biochemically and biologically. Molecular and cellular biology. 1999;19(2):1092-100. Epub 1999/01/16. PubMed PMID: 9891044; PubMed Central PMCID: PMC116039.

66. Ozeki C, Sawai Y, Shibata T, Kohno T, Okamoto K, Yokota J, et al. Cancer susceptibility polymorphism of p53 at codon 72 affects phosphorylation and degradation of p53 protein. The Journal of biological chemistry. 2011;286(20):18251-60. Epub 2011/04/02. doi: 10.1074/jbc.M110.208587. PubMed PMID: 21454683; PubMed Central PMCID: PMC3093897.

67. El Hallani S, Ducray F, Idbaih A, Marie Y, Boisselier B, Colin C, et al. TP53 codon 72 polymorphism is associated with age at onset of glioblastoma. Neurology. 2009;72(4):332-6. Epub 2009/01/28. doi: 10.1212/01.wnl.0000341277.74885.ec. PubMed PMID: 19171829.

68. Jones JS, Chi X, Gu X, Lynch PM, Amos CI, Frazier ML. p53 polymorphism and age of onset of hereditary nonpolyposis colorectal cancer in a Caucasian population. Clinical cancer research : an official journal of the American Association for Cancer Research. 2004;10(17):5845-9. Epub 2004/09/10. doi: 10.1158/1078-0432.CCR-03-0590. PubMed PMID: 15355915.

69. Kruger S, Bier A, Engel C, Mangold E, Pagenstecher C, von Knebel Doeberitz M, et al. The p53 codon 72 variation is associated with the age of onset of hereditary non-polyposis colorectal cancer (HNPCC). Journal of medical genetics. 2005;42(10):769-73. Epub 2005/10/04. doi: 10.1136/jmg.2004.028506. PubMed PMID: 16199549; PubMed Central PMCID: PMC1735929.

70. Pim D, Banks L. p53 polymorphic variants at codon 72 exert different effects on cell cycle progression. International journal of cancer Journal international du cancer. 2004;108(2):196-9. Epub 2003/11/26. doi: 10.1002/ijc.11548. PubMed PMID: 14639602.

71. Rogler A, Rogenhofer M, Borchardt A, Lunz JC, Knoell A, Hofstaedter F, et al. P53 codon 72 (Arg72Pro) polymorphism and prostate cancer risk: association between disease onset and proline genotype. Pathobiology : journal of immunopathology, molecular and cellular biology.

2011;78(4):193-200. Epub 2011/07/23. doi: 10.1159/000326767. PubMed PMID: 21778786.

72. Orsted DD, Bojesen SE, Tybjaerg-Hansen A, Nordestgaard BG. Tumor suppressor p53 Arg72Pro polymorphism and longevity, cancer survival, and risk of cancer in the general population. The Journal of experimental medicine. 2007;204(6):1295-301. Epub 2007/05/31. doi: 10.1084/jem.20062476. PubMed PMID: 17535973; PubMed Central PMCID: PMC2118619.

73. Chi SW, Lee SH, Kim DH, Ahn MJ, Kim JS, Woo JY, et al. Structural details on mdm2-p53 interaction. The Journal of biological chemistry. 2005;280(46):38795-802. Epub 2005/09/15. doi: 10.1074/jbc.M508578200. PubMed PMID: 16159876.

74. Daughdrill GW, Ackerman J, Isern NG, Botuyan MV, Arrowsmith C, Wold MS, et al. The weak interdomain coupling observed in the 70 kDa subunit of human replication protein A is unaffected by ssDNA binding. Nucleic acids research. 2001;29(15):3270-6. Epub 2001/07/27. PubMed PMID: 11470885; PubMed Central PMCID: PMC55822.

75. Pazgier M, Liu M, Zou G, Yuan W, Li C, Li J, et al. Structural basis for high-affinity peptide inhibition of p53 interactions with MDM2 and MDMX. Proceedings of the National Academy of Sciences of the United States of America. 2009;106(12):4665-70. Epub 2009/03/04. doi: 10.1073/pnas.0900947106. PubMed PMID: 19255450; PubMed Central PMCID: PMC2660734.

76. Schon O, Friedler A, Bycroft M, Freund SM, Fersht AR. Molecular mechanism of the interaction between MDM2 and p53. Journal of molecular biology. 2002;323(3):491-501. Epub 2002/10/17. PubMed PMID: 12381304.

77. Kussie PH, Gorina S, Marechal V, Elenbaas B, Moreau J, Levine AJ, et al. Structure of the MDM2 oncoprotein bound to the p53 tumor suppressor transactivation domain. Science. 1996;274(5289):948-53. Epub 1996/11/08. PubMed PMID: 8875929.

78. Teufel DP, Bycroft M, Fersht AR. Regulation by phosphorylation of the relative affinities of the N-terminal transactivation domains of p53 for p300 domains and Mdm2. Oncogene. 2009;28(20):2112-8. Epub 2009/04/14. doi: 10.1038/onc.2009.71. PubMed PMID: 19363523; PubMed Central PMCID: PMC2685776.

79. Teufel DP, Freund SM, Bycroft M, Fersht AR. Four domains of p300 each bind tightly to a sequence spanning both transactivation subdomains of

p53. Proceedings of the National Academy of Sciences of the United States of America. 2007;104(17):7009-14. Epub 2007/04/18. doi: 10.1073/pnas.0702010104. PubMed PMID: 17438265; PubMed Central PMCID: PMC1855428.

80. Phan J, Li Z, Kasprzak A, Li B, Sebti S, Guida W, et al. Structure-based design of high affinity peptides inhibiting the interaction of p53 with MDM2 and MDMX. The Journal of biological chemistry. 2010;285(3):2174-83. Epub 2009/11/17. doi: 10.1074/jbc.M109.073056. PubMed PMID: 19910468; PubMed Central PMCID: PMC2804373.

81. Li C, Pazgier M, Yuan W, Liu M, Wei G, Lu WY, et al. Systematic mutational analysis of peptide inhibition of the p53-MDM2/MDMX interactions. Journal of molecular biology. 2010;398(2):200-13. Epub 2010/03/17. doi: 10.1016/j.jmb.2010.03.005. PubMed PMID: 20226197; PubMed Central PMCID: PMC2856455.

82. Ferreon JC, Lee CW, Arai M, Martinez-Yamout MA, Dyson HJ, Wright PE. Cooperative regulation of p53 by modulation of ternary complex formation with CBP/p300 and HDM2. Proceedings of the National Academy of Sciences of the United States of America. 2009;106(16):6591-6. Epub 2009/04/10. doi: 10.1073/pnas.0811023106. PubMed PMID: 19357310; PubMed Central PMCID: PMC2672497.

83. Lee CW, Ferreon JC, Ferreon AC, Arai M, Wright PE. Graded enhancement of p53 binding to CREB-binding protein (CBP) by multisite phosphorylation. Proceedings of the National Academy of Sciences of the United States of America. 2010;107(45):19290-5. Epub 2010/10/22. doi: 10.1073/pnas.1013078107. PubMed PMID: 20962272; PubMed Central PMCID: PMC2984141.

84. Yin Y, Stephen CW, Luciani MG, Fahraeus R. p53 Stability and activity is regulated by Mdm2-mediated induction of alternative p53 translation products. Nature cell biology. 2002;4(6):462-7. Epub 2002/05/29. doi: 10.1038/ncb801. PubMed PMID: 12032546.

85. Zuiderweg ER. Mapping protein-protein interactions in solution by NMR spectroscopy. Biochemistry. 2002;41(1):1-7. Epub 2002/01/05. PubMed PMID: 11771996.

86. Cavanagh F, Palmer, and Skelton. Protein NMR spectroscopy Principles and Practice. 1st ed. San Diego, CA: Academic Press Inc; 2007.

87. Lum JK, Neuweiler H, Fersht AR. Long-Range Modulation of Chain Motions within the Intrinsically Disordered Transactivation Domain of Tumor Suppressor p53. Journal of the American Chemical Society.

2012;134(3):1617-22. Epub 2011/12/20. doi: 10.1021/ja2078619. PubMed PMID: 22176582; PubMed Central PMCID: PMC3265989.

Appendix 1: M9 Minimal Media Recipe

Stock Solutions:

1. 1 liter of 10X M9 Salts

Na2HPO4	60g
KH2PO4	30g
NaCl	5g

2. 1M MgSO4 Filter sterilized
3. 20% Dextrose Filter Sterilized
4. 50mM CaCl2 Filter Sterilized
5. 0.01 FeCl3 (in 0.1M HCL to prevent precipitation)
6. 5mg/ml Vitamin B1 Filter Sterilized

To make 2 liters of M9 Media, to 1.7 liters of ddH_20

- 200ml of 10X M9 Salts
- 4ml 1M MgSO4
- 20 ml of 20% D-Glucose (or 2g/l of dry glucose)
- 4ml of 50mM CaCl2
- 2ml 0.01M FeCl3
- 400µl of 5mg/ml Vitamin B1
- pH to 7.3-7.5
- QS to 2 liters with ddH_20

Appendix 2: ^{15}N labeled RPAΔ122 ^{1}H-^{15}N chemical shifts from titration with ^{14}N human p53TAD74Δ72R.

	[0mM]		[0.065mM]		[0.126mM]	
Residue	H shift	N shift	H shift	N shift	H shift	N shift
G3	8.49472	112.60674	8.49877	112.57875	8.49545	112.5707
Q4	8.05931	118.70228	8.06646	118.7038	8.0658	118.70276
L5	8.10679	118.70406	8.11058	118.70214	8.11278	118.70189
S6	9.10108	118.21407	9.11024	118.21766	9.11916	118.24112
E7	7.82985	126.62897	7.83498	126.66325	7.83641	126.64723
G8	7.46378	112.62811	7.46808	112.63383	7.44658	112.37222
A9	8.61853	126.06001	8.62634	126.03616	8.63234	126.02344
I10	8.97124	117.1506	8.97618	117.15587	8.96836	117.12127
A11	8.47768	122.23817	8.48586	122.22247	8.49624	122.19742
A12	7.87684	120.11706	7.88321	120.11942	7.87658	119.9857
I13	8.33613	119.40733	8.34114	119.3989	8.33213	119.46397
M14	7.95402	114.6039	7.95912	114.66241	7.95911	114.81184
Q15	8.7774	117.85872	8.77922	117.84295	8.76431	117.73307
K16	7.67131	116.01237	7.67732	116.01322	7.68725	116.12341
G17	7.68825	108.8917	7.69666	108.89277	7.732782	108.97016
D18	7.47496	119.41606	7.48031	119.41169	7.43457	119.25576
T19	7.96514	113.01614	7.96775	112.95087	7.94901	112.87827
N20	8.75985	121.67473	7.86119	121.64814	8.75115	121.62254
I21	7.21755	115.59309	7.2199	115.58829	7.2112	115.44206
K22	8.36592	122.38187	8.37018	122.3791	8.37392	122.29372
I24	9.08966	121.67828	9.09648	121.69381	9.10138	121.69863
L25	8.60123	123.65409	8.60883	123.64906	8.61151	123.64106
Q26	9.40683	119.97401	9.41479	119.98541	9.42011	120.02401
V27	8.78953	127.40601	8.79253	127.40748	8.76625	127.40642
I28	9.38958	128.74265	9.39216	128.77696	9.37224	128.75554
N29	7.7768	114.62202	7.78264	114.7016	7.78081	114.79806
I30	8.31274	121.10027	8.31537	121.09098	8.3041	121.2686
R31	9.18069	127.32478	9.19097	127.32424	9.19426	127.35426
I33	9.08939	123.76946	9.08693	123.76572	9.0386	123.95855
T34	8.39506	119.57108	8.3936	119.57032	8.35812	119.38955
T35	8.39418	117.14801	8.39551	117.13085	8.35456	116.87991
G36	8.60115	112.60674	8.60271	112.53287	8.58115	112.3444
R41	7.64153	118.27394	7.64559	118.3233	7.62836	118.40776
Y42	9.26557	120.25946	9.26979	120.23985	9.27029	120.12081
R43	8.88943	124.36253	8.89065	124.40101	8.86804	124.35854

	[0mM]		[0.065mM]		[0.126mM]	
Residue	H shift	N shift	H shift	N shift	H shift	N shift
L44	9.15114	127.19112	9.1509	127.2118	9.12687	127.35183
L45	8.1127	123.94019	8.12221	123.93026	8.15975	123.65063
M46	8.25318	122.52427	8.26	122.50504	8.25759	122.55097
S47	8.9417	112.62324	8.94151	112.61787	8.91918	112.49933
D48	8.74154	127.26814	8.75306	127.26392	8.74027	127.26095
G49	8.86554	107.39132	8.87191	107.38456	8.88047	107.40484
L50	8.50147	121.95661	8.50768	121.98894	8.49883	121.95937
N51	10.21852	118.86313	10.22463	118.88677	10.21568	188.83913
T52	7.65369	105.83672	7.66308	105.87403	7.67868	105.93496
L53	8.47126	119.98016	8.47668	120.00486	8.47375	119.84361
S54	9.0129	121.51517	9.02872	121.48524	9.11794	121.4344
S55	6.93034	116.01674	6.9408	116.15755	6.994	117.24545
F56	7.17094	117.57133	7.18402	117.59602	7.30784	117.174
M57	9.41832	121.10448	9.42155	121.09737	9.39154	121.08389
A59	8.52449	131.29565	8.52701	131.27145	8.49283	130.58478
T60	8.50058	115.88895	8.50758	115.89041	8.52354	115.87483
Q61	9.0002	120.54276	9.00761	120.52618	9.02969	120.52987
L62	8.0537	117.43435	8.0599	117.46102	8.05536	117.46824
N63	7.80051	122.24356	7.80677	122.26669	7.81207	122.26233
L65	7.93014	113.36299	7.93235	113.32162	7.91347	113.29031
V66	7.38864	118.70502	7.39822	118.74209	7.40936	118.9766
E67	7.82516	121.95584	7.83144	121.97433	7.82516	121.97812
E68	8.30668	114.88316	8.31067	114.84889	8.29029	114.81021
E69	7.54763	112.91103	7.55258	112.9156	7.54515	112.45525
Q70	7.80464	116.44814	7.80919	116.49712	7.81155	116.51871
L71	7.3588	119.78008	7.36499	199.80554	7.37173	120.00371
S72	7.24815	117.15189	7.25251	117.20356	7.25251	117.33606
S73	8.68356	118.14029	8.69112	118.15598	8.69559	118.25958
N74	8.81857	114.7481	8.82975	114.75043	8.84915	114.72945
C75	8.15422	117.56303	8.16327	117.5332	8.17541	117.54194
V76	8.54825	120.82168	8.55217	120.8192	8.54261	120.74581
C77	9.32232	122.80442	9.32878	122.8052	9.33461	122.80572
Q78	9.11577	120.82077	9.12058	120.78825	9.11786	120.786
I79	8.71311	127.0759	8.73044	127.17488	8.72513	127.17561
H80	7.99996	124.50445	8.00769	124.49002	8.01462	124.50413
R81	7.85875	117.71114	7.8654	117.68836	7.87373	117.69311
F82	8.83636	125.35076	8.84688	125.34533	8.86818	125.35273
I83	8.73023	116.73206	8.73974	116.81507	8.75632	119.91483
V84	8.71229	124.50558	8.71898	124.48707	8.71629	124.33618
T86	8.54826	118.56321	8.55637	118.58945	8.57126	118.94386
L87	9.11248	127.86527	9.11689	127.8339	9.10833	127.49507
K88	8.5768	120.92942	8.58491	120.89823	8.55897	120.9244
D89	7.72444	115.37907	7.73129	115.34027	7.74512	115.16412
G90	8.06578	108.09757	8.07153	108.16183	8.05848	108.25146
R91	7.75402	121.24566	7.7653	121.2571	7.8049	121.39096
R92	8.36494	120.12046	8.36809	120.18205	8.29969	120.37558

	[0mM]		[0.065mM]		[0.126mM]	
Residue	H shift	N shift	H shift	N shift	H shift	N shift
V93	8.74884	118.84773	8.7475	118.82851	8.76421	117.73307
V94	8.09492	124.79263	8.10435	124.82636	8.11725	124.79695
I95	9.36544	127.66432	9.37457	127.68437	9.38064	127.68185
L96	9.08334	126.19267	9.09007	126.19371	9.09431	126.22703
M97	8.21827	120.5441	8.22018	120.55229	8.21046	120.40545
L99	8.78324	123.79875	8.78596	123.78936	8.75749	123.63207
E100	8.75496	120.34846	8.75496	120.34865	8.75333	120.32056
V101	9.40726	127.75901	9.40613	127.60266	9.39926	127.68217
L102	8.94548	129.67847	8.95155	129.67819	8.95431	129.68576
K103	7.75339	117.57032	7.75764	117.58583	7.74959	117.56532
S104	8.74073	120.33979	8.74073	120.33979	8.73921	120.28172
A105	8.74204	123.08772	8.75254	123.10425	8.77412	123.10271
E106	8.56553	117.2826	8.5686	117.26859	8.5665	117.26879
A107	7.67092	121.95584	7.67584	121.9607	7.6757	121.96309
V108	7.71817	118.5846	7.72578	118.62908	7.73335	118.66089
G109	8.22418	106.82076	8.23033	106.76716	8.23224	106.7403
V110	7.13564	114.89161	7.14198	114.9081	7.14138	114.89805
K111	8.03568	123.0874	8.03991	123.11765	8.0369	123.10342
I112	9.21767	130.302	9.22344	130.30597	9.23173	130.33345
G113	8.33	114.30955	8.33384	114.27973	8.32746	114.28344
N114	8.45973	116.01383	8.46373	116.01685	8.46112	116.02251
V116	8.06063	116.02081	8.06549	118.97226	8.05298	115.7333
Y118	9.13634	125.92437	9.13713	125.90623	9.09501	125.53538
N119	7.93582	125.977	7.94034	125.97516	7.94396	125.9465
E120	8.23864	124.21947	8.23964	124.19786	8.31426	124.25186
G121	7.93297	115.30896	7.93677	115.32671	7.92596	115.44406

	[0.165mM]		[0.186mM]		[0.198mM]	
Residue	H shift	N shift	H shift	N shift	H shift	N shift
G3	8.49545	112.5707	8.49273	112.57123	8.4932	112.58458
Q4	8.0658	118.70276	8.0658	118.70276	8.06249	118.70398
L5	8.11278	118.70189	8.11278	118.70189	8.11164	118.70398
S6	9.11914	118.28088	9.11914	118.28088	9.11794	118.27278
E7	7.83641	126.64723	7.8333	126.62824	7.83462	126.62774
G8	7.44658	112.37222	7.4475	112.3442	7.45331	112.34521
A9	8.63234	126.02344	8.6298	126.05714	8.63144	126.0541
I10	8.96428	117.14502	8.96428	117.14502	8.95943	117.12668
A11	8.49666	122.23648	8.49499	122.234	8.49868	122.23129
A12	7.87658	119.9857	7.87158	119.97449	7.87205	119.97836
I13	8.32393	119.49432	8.32393	119.49432	8.32127	119.53873
M14	7.9595	114.89787	7.95551	114.89851	7.96032	114.88825
Q15	8.7603	117.72203	8.7532	117.71851	8.7532	117.71851
K16	7.68725	116.12341	7.68725	116.12341	7.68725	116.12341
G17	7.74643	108.99072	7.74721	108.99042	7.74794	108.9912
D18	7.43457	119.25576	7.45569	119.25188	7.45702	119.25705
T19	7.9399	112.85008	7.9399	112.85008	7.93916	112.78754

	[0.165mM]		[0.186mM]		[0.198mM]	
Residue	H shift	N shift	H shift	N shift	H shift	N shift
N20	8.74736	121.69197	8.74285	121.61817	8.74223	121.61871
I21	7.2112	115.44206	7.20621	115.41461	7.20633	115.39547
K22	8.37433	122.26398	8.37104	122.24689	8.37338	122.24426
I24	9.10097	121.67191	9.10097	121.67191	9.10097	121.67191
L25	8.60912	123.65765	8.60912	123.65765	8.60912	123.65765
Q26	9.4184	120.02338	9.4184	120.02338	9.4184	120.02338
V27	8.75424	127.41192	8.75424	127.41192	8.75122	127.44817
I28	9.37018	128.75157	9.36083	128.74648	9.36083	128.74648
N29	7.77672	114.8571	7.77513	114.85713	7.77196	114.86937
I30	8.29853	121.28085	8.29444	121.36154	8.29444	121.36154
R31	9.18943	127.33842	9.18943	127.33842	9.18943	127.33842
I33	9.0276	124.00481	9.01826	124.07225	9.01328	124.07375
T34	8.35014	119.30526	8.34748	119.28164	8.34685	119.2874
T35	8.3459	116.85824	8.34183	116.85817	8.33654	116.85831
G36	8.57248	112.2991	8.57112	112.2998	8.56816	112.24475
R41	7.62196	118.42001	7.61777	118.41187	7.61777	118.41187
Y42	9.26678	120.12093	9.26678	120.12093	9.27127	120.11524
R43	8.86009	124.35056	8.85423	124.362	8.85521	124.36099
L44	9.13514	127.35757	9.13514	127.35757	9.13514	127.35757
L45	8.1459	123.67451	8.1459	123.67451	8.14348	123.63243
M46	8.2542	122.52785	8.2542	122.52785	8.2542	122.52785
S47	8.91315	112.4857	8.9066	112.48395	8.9066	112.48395
D48	8.73445	127.26607	8.73445	127.26607	8.73672	127.26476
G49	8.877	107.39162	8.88057	107.3903	8.88057	107.3903
L50	8.495	121.95755	8.48946	121.95736	8.49151	121.96056
N51	10.21239	118.83825	10.20664	118.83381	10.20791	118.83395
T52	7.68546	105.93919	7.68069	105.93968	7.68371	105.97414
L53	8.47066	119.83709	8.4705	119.83289	8.4705	119.83289
S54	9.13542	121.3974	9.1367	121.39838	9.14537	121.39046
S55	6.99462	117.43574	7.00123	117.54698	7.00295	117.5771
F56	7.30784	117.174	7.31146	117.1496	7.31733	117.14792
M57	9.3815	121.10734	9.37737	121.09971	9.37672	121.09631
A59	8.48299	130.44594	8.4474	130.44615	8.47659	130.3017
T60	8.52397	115.87118	8.52397	115.87118	8.52399	115.86612
Q61	9.03391	120.52967	9.03109	120.52777	9.0613	120.53278
L62	8.05288	117.46864	8.04778	117.43398	8.04778	117.43398
N63	7.81207	122.26233	7.80733	122.2562	7.81339	122.27343
L65	7.90578	113.28272	7.90037	113.28274	7.90297	113.2806
V66	7.40607	118.97706	7.40898	118.97608	7.40868	119.09051
E67	7.82516	121.97812	7.81791	122.05606	7.81791	122.05608
E68	8.2832	114.80456	8.2796	114.77894	8.2772	114.75609
E69	7.54515	112.45525	7.5453	112.47873	7.5453	112.47873
Q70	7.81155	116.51871	7.81155	116.51871	7.80721	116.52219
L71	7.37162	120.10326	7.36536	120.10297	7.37138	120.11861
S72	7.24724	117.41167	7.24778	117.42372	7.24834	117.42976
S73	8.69559	118.25958	8.69473	118.25884	8.69473	118.25884
N74	8.85069	114.74072	8.85069	114.74072	8.85324	114.74126

	[0.165mM]		[0.186mM]		[0.198mM]	
Residue	H shift	N shift	H shift	N shift	H shift	N shift
C75	8.17923	117.56538	8.17658	117.56313	8.17658	117.56313
V76	8.53589	120.68551	8.53589	120.68551	8.53589	120.68551
C77	9.33461	122.80572	9.33461	122.80572	9.33461	122.80572
Q78	9.11579	120.82922	9.11228	120.81113	9.11228	120.81113
I79	8.72258	127.19044	8.72258	127.19044	8.71794	127.12451
H80	8.01462	124.50413	8.01283	124.50343	8.01762	124.50292
R81	7.87373	117.69311	7.87101	117.69481	7.8751	117.71111
F82	8.87603	125.35317	8.87148	125.35436	8.87148	125.35436
I83	8.7593	116.96954	8.7593	116.96954	8.7593	116.96954
V84	8.71501	124.22902	8.71149	124.22007	8.71149	124.22007
T86	8.5717	118.99638	8.5717	118.99638	8.5717	118.99638
L87	9.10833	127.49507	9.09996	127.49565	9.09998	127.34804
K88	8.5721	121.07577	8.56579	121.07684	8.57013	121.07457
D89	7.74759	115.16305	7.74759	115.16305	7.74759	115.16305
G90	8.05848	108.25146	8.05041	108.25367	8.05041	108.25367
R91	7.81659	121.39577	7.81262	121.39215	7.81717	121.3908
R92	8.27994	120.37433	8.27764	120.40013	8.27225	120.40246
V93	8.65951	118.6536	8.65435	118.64227	8.65345	118.58379
V94	8.11725	124.79695	8.11725	124.79695	8.11725	124.79695
I95	9.38064	127.68185	9.38064	127.68185	9.38064	127.68185
L96	9.09431	126.22703	9.09431	126.22703	9.09431	126.22703
M97	8.20701	120.37859	8.20701	120.37859	8.20701	120.37859
L99	8.74798	123.5997	8.74798	123.5997	8.74366	123.51326
E100	8.75333	120.32056	8.75333	120.32056	8.75333	120.32056
V101	9.39926	127.68217	9.39926	127.68217	9.39926	127.68217
L102	8.95431	129.68576	8.95029	129.70605	8.95226	129.71947
K103	7.74145	117.55917	7.74145	117.55917	7.7418	117.56816
S104	8.73921	120.28172	8.73921	120.28172	8.73921	120.28172
A105	8.77706	123.08849	8.77706	123.08849	8.78333	123.07632
E106	8.5665	117.26879	8.56364	117.26866	8.56426	117.27957
A107	7.6757	121.96309	7.67153	121.95955	7.67153	121.95955
V108	7.73335	118.66089	7.73057	118.65158	7.73057	118.65158
G109	8.23224	106.7403	8.23072	106.73915	8.23014	106.69326
V110	7.14138	114.89805	7.13644	114.88908	7.13555	114.88841
K111	8.03397	123.06836	8.03077	123.06593	8.03092	123.0893
I112	9.23002	130.30272	9.23002	130.30272	9.23002	130.30272
G113	8.32487	114.28533	8.32091	114.28402	8.32393	114.28932
N114	8.46112	116.02251	8.46112	116.02251	8.4569	116.02289
V116	8.04755	115.67507	8.04755	115.67507	8.04759	115.60922
Y118	9.08397	125.47266	9.08054	125.47309	9.07717	125.38454
N119	7.94396	125.9465	7.94396	125.9465	7.94376	125.9184
E120	8.31079	124.37102	8.30635	124.37193	8.30612	124.49686
G121	7.92252	115.4482	7.92252	115.4482	7.92252	115.4482

	[0.293mM]		[.3185mM]		[0.357mM]	
Residue	H shift	N shift	H shift	N shift	H shift	N shift
G3	8.48918	112.57901	8.48918	112.57901	8.48381	112.58531
Q4	8.06042	118.70712	8.06476	118.70566	8.05957	118.70909
L5	8.11164	118.70396	8.11254	118.70238	8.10689	118.70228
S6	9.11939	118.28086	9.1248	118.27842	9.11852	118.27683
E7	7.8361	126.628	7.8361	126.628	7.82995	126.63061
G8	7.45954	112.33442	7.45954	112.33442	7.45405	112.33369
A9	8.6307	126.05193	8.63532	126.05704	8.63035	126.05887
I10	8.95943	117.12668	8.95935	117.07037	8.954	117.06158
A11	8.49796	122.2376	8.49984	122.24172	8.49793	122.23441
A12	7.87125	119.97802	7.87125	119.97802	7.8667	119.96715
I13	8.31825	119.53418	8.32104	119.55587	8.31276	119.55148
M14	7.95416	114.8933	7.95873	114.88215	7.95407	114.88773
Q15	8.75097	117.71367	8.75138	117.71338	8.74805	117.71225
K16	7.69125	116.15827	7.69208	116.15403	7.67914	116.15489
G17	7.7594	109.06181	7.76061	109.0592	7.76325	109.07111
D18	7.45942	119.26151	7.46507	119.28349	7.44699	119.28018
T19	7.92992	112.76955	7.93432	112.76987	7.923432	112.76807
N20	8.74223	121.61871	8.74197	121.61446	8.73751	121.60032
I21	7.20107	115.31134	7.20453	115.31332	7.19931	115.31136
K22	8.37186	122.24417	8.37484	122.24827	8.37037	122.25004
I24	9.10097	121.67191	9.09987	121.67371	9.09505	121.67797
L25	8.60912	123.65765	8.61249	123.66027	8.607	123.6505
Q26	9.41844	120.0659	9.42353	120.07526	9.41858	120.11265
V27	8.74837	127.45145	8.74825	127.43205	8.74211	127.42564
I28	9.35512	128.74992	9.3541	128.74861	9.34976	128.7431
N29	7.77196	114.86937	7.77148	114.86987	7.76731	114.88219
I30	8.29444	121.36154	8.29444	121.36154	8.28892	121.39593
R31	9.18943	127.33842	9.19517	127.33973	9.18822	127.33759
I33	9.00666	124.07865	9.00418	124.08161	9.00057	124.0826
T34	8.34169	119.27202	9.34195	119.26221	8.33588	119.26147
T35	8.32911	116.73598	8.32911	116.73598	8.32417	116.72891
G36	8.56531	122.20745	8.56531	122.20745	8.55935	112.19471
R41	7.6128	118.4287	7.6157	118.4336	7.61318	118.436
Y42	9.26591	120.11846	9.2663	119.97427	9.25995	119.9826
R43	8.84867	124.35641	8.85273	124.35989	8.8469	124.35699
L44	9.13514	127.35757	9.14221	127.41045	9.15718	127.40204
L45	8.14255	123.55729	8.14705	123.49854	8.14196	123.50988
M46	8.25445	122.59405	8.2543	122.61494	8.2485	122.60418
S47	8.90086	112.47749	8.90111	112.47687	8.89603	112.48212
D48	8.73672	127.26478	8.7316	127.27294	8.72549	127.26451
G49	8.88057	107.3903	8.8833	107.39097	8.8833	107.39097
L50	8.4891	121.9623	8.4898	121.95035	8.48593	121.94537
N51	10.20759	118.83279	10.20699	118.84419	10.20157	118.84206
T52	7.68335	105.97404	7.68969	105.97995	7.68262	105.97832
L53	8.46663	119.71126	8.47066	119.70908	8.46558	119.69682
S54	9.15987	121.39642	9.16516	121.38496	9.16703	121.38502
S55	7.01212	117.7034	7.01814	117.84956	7.01851	117.85889

	[0.293mM]		[.3185mM]		[0.357mM]	
Residue	H shift	N shift	H shift	N shift	H shift	N shift
F56	7.33595	117.11839	7.34331	117.01931	7.34223	117.01437
M57	9.37113	121.10075	9.37113	121.10075	9.36623	121.0037
A59	8.47172	130.16588	8.47114	130.16701	8.46543	130.1665
T60	8.53046	115.86622	8.53012	115.87691	8.53012	115.87691
Q61	9.03997	120.53897	9.04204	120.5462	9.03821	120.53872
L62	8.04778	117.43398	8.05371	117.4449	8.04756	117.44371
N63	7.8129	122.27144	7.81111	122.25417	7.80608	122.25101
L65	7.89457	113.27416	7.89797	113.20464	7.88905	113.20034
V66	7.40868	119.09051	7.40927	119.12634	7.40082	119.12556
E67	7.81791	122.05608	7.8196	122.07246	7.81332	122.08224
E68	8.2772	114.75609	8.2772	114.75609	8.27162	114.74988
E69	7.5453	112.47873	7.5453	112.47873	7.5403	112.47773
Q70	7.80653	116.56302	7.81163	116.56654	7.80556	116.57528
L71	7.37138	120.11861	7.37406	120.11799	7.36641	120.12436
S72	7.24669	117.42654	7.24669	117.42654	7.24179	117.41978
S73	8.69488	118.25573	8.69653	118.27384	8.69094	118.30238
N74	8.85704	114.74201	8.85959	114.74072	8.85986	114.74093
C75	8.18033	117.56304	8.18243	117.56407	8.17724	117.53307
V76	8.53254	120.68336	8.53556	120.68338	8.53065	120.67885
C77	9.33661	122.80743	9.33741	122.80711	9.33052	122.80355
Q78	9.11228	120.81113	9.11293	120.79371	9.10641	120.77634
I79	8.71794	127.12451	8.71958	127.12366	8.71399	127.13269
H80	8.01145	124.49834	8.01833	124.50459	8.01833	124.50459
R81	7.87618	117.71252	7.87618	117.71252	7.87069	117.71323
F82	8.87706	125.3571	8.8796	125.35186	8.87735	125.35237
I83	8.76588	116.99091	8.76604	116.98788	8.76025	116.9763
V84	8.71149	124.22007	8.71236	124.22173	8.70593	124.21296
T86	8.57268	119.329	8.57625	119.13256	8.57155	119.12752
L87	9.09998	127.34804	9.10304	127.3358	9.09729	127.33222
K88	8.57046	121.0743	8.57046	121.0743	8.56912	121.09012
D89	7.75432	115.03851	7.75567	115.02457	7.7532	115.04819
G90	8.04762	108.3054	8.04762	108.3054	8.04217	108.30287
R91	7.82414	121.40808	7.8249	121.40952	7.82469	121.5022
R92	8.26004	120.49084	8.26004	120.49084	8.24822	120.54686
V93	8.63667	118.58425	8.63594	118.56979	8.6285	118.57613
V94	8.12383	124.78515	8.12383	124.78515	8.1187	124.78487
I95	9.38064	127.68185	9.38064	127.68185	9.37415	127.6154
L96	9.09385	126.23492	9.09651	126.29472	9.09409	126.29795
M97	8.20111	120.28157	8.20022	120.28413	8.19582	120.25977
L99	8.73583	123.51589	8.73589	123.51131	8.73067	123.51248
E100	8.75333	120.32056	8.74448	120.39692	8.73922	120.40055
V101	9.39926	127.68217	9.39926	127.68217	9.41235	127.69873
L102	8.95226	129.71947	8.95408	129.71849	8.94788	129.72952
K103	7.7371	117.56961	7.74196	117.56538	7.73536	114.57538
S104	8.73921	120.28172	8.73921	120.32193	8.73323	120.26759
A105	8.78341	123.09702	8.78985	123.08506	8.78295	123.08804
E106	8.56426	117.29315	8.56426	117.29315	8.55974	117.27934

	[0.293mM]		[.3185mM]		[0.357mM]	
Residue	H shift	N shift	H shift	N shift	H shift	N shift
A107	7.6743	121.96017	7.6743	121.96017	7.66968	121.95921
V108	7.73057	118.65158	7.7336	118.69747	7.73041	118.70372
G109	8.23014	106.69326	8.23014	106.69326	8.22388	106.69801
V110	7.13555	114.88841	7.13885	114.88706	7.13552	114.88171
K111	8.03092	123.0893	8.0333	123.09063	8.02976	123.08657
I112	9.23575	130.2959	9.23524	130.3091	9.23126	130.30403
G113	8.31901	114.30688	8.32202	114.32118	8.31807	114.32217
N114	8.4569	116.02289	8.45837	116.01915	8.45377	116.02079
V116	8.04225	115.59976	8.04225	115.59976	8.04094	115.58772
Y118	9.07065	125.34921	9.07112	125.35186	9.06541	125.35026
N119	7.94376	125.9184	7.94132	125.92151	7.94238	125.9246
E120	8.30147	124.59592	8.30162	124.63653	8.29405	124.64327
G121	7.92252	115.4482	7.91893	115.46407	7.91281	115.47981

	[0.416mM]		[0.5mM]	
Residue	H shift	N shift	H shift	N shift
G3	8.48489	112.56483	8.48914	112.51387
Q4	8.0626	118.70132	8.064466	118.70331
L5	8.11218	118.70444	8.11247	118.70626
S6	9.11931	118.27807	9.12481	118.28288
E7	7.83564	126.62865	7.83575	126.63704
G8	7.45977	112.34584	7.45926	112.34627
A9	8.63605	126.05061	8.63605	126.05061
I10	8.95368	117.03835	8.95968	117.08467
A11	8.5015	122.21987	8.50104	122.22164
A12	7.87065	119.91552	7.87086	119.9152
I13	8.31752	119.55891	8.31916	119.5562
M14	7.95414	114.87699	7.95929	114.89988
Q15	8.74837	117.69604	8.75049	117.69858
K16	7.69076	116.16357	7.69479	116.15222
G17	7.76575	109.08082	7.76972	109.08298
D18	7.46781	119.35693	7.45891	119.28732
T19	7.92975	112.77013	7.93027	112.76878
N20	8.73751	121.60032	8.73751	121.60032
I21	7.20196	115.30927	7.20089	115.3087
K22	8.37176	122.23462	8.37725	122.24618
I24	9.10581	121.68383	9.1012	121.69132
L25	8.61249	123.66027	8.61315	123.65929
Q26	9.42113	120.09075	9.42417	120.09886
V27	8.73744	127.42881	8.74242	127.42792
I28	9.3541	128.74861	9.35755	128.7494
N29	7.77067	114.88463	7.77025	114.89363
I30	8.28888	121.39385	8.29486	121.39775
R31	9.18959	127.33112	9.19536	127.33896

	[0.416mM]		[0.5mM]	
Residue	H shift	N shift	H shift	N shift
I33	9.00173	124.12769	9.00086	124.087
T34	8.33642	119.23441	8.33642	119.23441
T35	8.32169	116.72963	8.32409	116.73325
G36	8.5596	112.20389	8.5596	112.20389
R41	7.61139	118.42401	7.61388	118.4264
Y42	9.27252	119.98667	9.27252	119.98667
R43	8.84864	124.36092	8.84864	124.36092
L44	9.13322	127.41666	9.13071	127.5387
L45	8.14788	123.5356	8.1477	123.52261
M46	8.25344	122.65648	8.25949	122.6666
S47	8.90202	112.48276	8.90055	112.48398
D48	8.71717	127.25389	8.72682	127.28009
G49	8.8833	107.39097	8.88317	107.39787
L50	8.48836	121.96027	8.48836	121.96027
N51	10.20416	118.8273	10.20749	118.83269
T52	7.68969	105.97995	7.68807	105.97688
L53	8.46629	119.69462	8.47127	119.70194
S54	9.17726	121.38188	9.17791	121.39032
S55	7.02293	117.99625	7.02402	117.99348
F56	7.35654	117.00815	7.35889	117.01522
M57	9.36492	121.08514	9.36615	121.1027
A59	8.46487	130.16075	8.46621	130.13411
T60	8.53012	115.87691	8.53314	115.87337
Q61	9.04294	120.54892	9.04771	120.54293
L62	8.04668	117.42879	8.05152	117.43699
N63	7.81111	122.25417	7.81111	122.25417
L65	7.89535	113.19493	7.89495	113.19946
V66	7.40329	119.12925	7.40172	119.13563
E67	7.81918	122.05762	7.81918	122.05762
E68	8.27158	114.75621	8.27158	114.75621
E69	7.54415	112.47911	7.542	112.48576
Q70	7.81226	116.56062	7.81226	116.56062
L71	7.3714	120.12359	7.37789	120.14838
S72	7.2489	117.42619	7.24837	117.43728
S73	8.6949	118.28917	8.6949	118.28917
N74	8.8601	114.72706	8.8661	114.74685
C75	8.18282	117.5527	8.18382	117.57619
V76	8.536	120.68532	8.52992	120.686
C77	9.33635	122.81353	9.33635	122.81353
Q78	9.10676	120.79881	9.11308	120.76868
I79	8.71891	127.0814	8.71873	127.05315
H80	8.02113	124.506	8.02113	124.506
R81	7.8772	117.71114	7.87797	117.71732
F82	8.88157	125.35076	8.88308	125.35028
I83	8.76611	117.00624	8.76611	117.00624
V84	8.70677	124.20631	8.71253	124.2204

	[0.416mM]		[0.5mM]	
Residue	H shift	N shift	H shift	N shift
T86	8.57738	119.17541	8.57714	119.21103
L87	9.09652	127.33701	9.10069	127.32381
K88	8.56609	121.09295	8.57145	121.09303
D89	7.75844	115.01825	7.75958	115.04354
G90	8.04329	108.34087	8.04814	108.38067
R91	7.8304	121.50509	7.82982	121.53538
R92	8.24785	120.54215	8.2482	120.54296
V93	8.62892	118.57237	8.63043	118.57333
V94	8.12441	124.7656	8.1242	124.78152
I95	9.37245	127.62317	9.37737	127.62215
L96	9.09562	126.2972	9.09896	126.3353
M97	8.19437	120.25808	8.19437	120.25808
L99	8.73095	123.50819	8.73637	123.51622
E100	8.74096	120.40315	8.74234	120.40031
V101	9.41111	127.69692	9.44034	127.73339
L102	8.94877	129.7179	8.9545	129.73732
K103	7.74156	117.54368	7.7413	117.57744
S104	8.73307	120.21799	8.72941	120.16267
A105	8.78938	123.08546	8.79021	123.08703
E106	8.56504	117.28217	8.56504	117.28217
A107	7.67194	121.94656	7.67118	121.95902
V108	7.736	118.69333	7.73617	118.70895
G109	8.22995	106.69196	8.22991	106.68785
V110	7.1391	114.87959	7.13991	114.8923
K111	8.03058	123.09205	8.03058	123.09205
I112	9.23172	130.30148	9.24244	130.39037
G113	8.31853	114.31683	8.31853	114.31683
N114	8.45377	116.02079	8.45981	116.02187
V116	8.04058	115.54128	8.04161	115.57133
Y118	9.06532	125.3315	9.06568	125.34258
N119	7.94245	125.92411	7.94711	125.92171
E120	8.30146	124.64153	8.30194	124.64891
G121	7.915	115.46492	7.91736	115.51824

Appendix 3: ^{15}N labeled p53TAD74Δ72R ^{1}H-^{15}N chemical shifts and peak intensity upon titration with ^{14}N MDM2 (17-125).

	[0mm]			[.005mM]		
Residue	H shift	N shift	Intensity	H shift	N shift	Intensity
M1	8.38921	121.57822	0.3472	8.38922	121.61005	0.3421
E2	8.35346	122.1015	0.7653	8.35376	122.09689	0.7303
E3	8.38897	123.54234	1.1073	8.38902	123.53931	1.1221
Q5	8.5188	121.03509	0.5245	8.51859	121.03289	0.5085
S6	8.34222	117.75684	0.2494	8.34203	117.75394	0.2596
D7	8.40081	123.68549	0.7176	8.40114	123.68714	0.224
S9	8.48325	116.01997	0.5015	8.49109	116.01869	0.4778
V10	7.82659	121.13232	0.7326	7.82786	121.12839	0.6974
E11	8.2953	126.14723	0.9371	8.30669	126.14424	0.9026
L14	8.3068	122.45206	0.8937	8.3068	122.45175	0.9485
S15	8.28796	116.69543	0.3432	8.29062	116.69282	0.3589
S15'	8.35092	116.87386	0.0034	8.35085	116.86983	0.0002
Q16	8.44366	122.54105	0.3246	8.44761	122.56557	0.3461
E17	8.43434	121.99925	0.4095	8.43312	121.99965	0.4081
T18	8.07143	114.87696	0.3718	8.07146	114.86373	0.363
T18'	8.39015	113.50847	-0.002	8.39738	113.99001	-0.0013
F19	8.20094	122.29047	0.3962	8.20078	122.28687	0.3803
F19'	8.14317	123.14242	-0.0107	8.14566	123.45153	-0.00331
S20	8.06274	116.74464	0.144	8.06435	116.74104	0.138
S20'	7.94758	117.15224	-0.0002	7.94661	17.17829	0.0005
D21	8.23645	122.0976	0.2773	8.23641	122.09476	0.2605
D21'	8.11853	121.42062	0.1096	8.1185	121.4181	0.1125
L22	7.90673	121.13192	1.0496	7.90667	121.12881	1.0396
W23	7.81259	119.39646	1.0447	7.81271	119.39336	0.9801
W23'	7.76807	119.39822	-0.0064	7.75992	119.39823	0.0099
K24	7.55257	120.45626	0.7276	7.55367	120.45707	0.7176
K24'	7.30116	120.16179	-0.0008	7.30094	120.16608	0.0036
L25	7.78891	120.74577	0.8411	7.7891	120.74264	0.8415
L25'	7.90678	120.64973	0.0071	7.90213	123.64848	0.0009
L26	7.86848	123.72094	0.9005	7.87155	123.73322	0.8737
E28	8.67161	119.7818	0.9334	8.67164	119.77941	0.9159
N29	8.23656	118.81824	0.3126	8.23951	118.81547	0.2835
N29'	8.24059	119.09757	0.0117	8.2477	119.10239	0.016
N30	8.24768	119.58994	0.2065	8.24814	119.58644	0.1975
V31	7.98906	120.16756	0.7136	7.98911	120.16735	0.658

	[0mm]			[.005mM]		
Residue	H shift	N shift	Intensity	H shift	N shift	Intensity
L32	8.24855	125.47619	0.8143	8.24824	125.46992	0.7849
S33	8.17734	118.05961	0.5061	8.17735	118.04543	0.4694
S33'	8.17697	118.33422	0.03	8.17751	118.33214	0.0351
L35	8.25967	123.73632	1.0871	8.25973	123.7327	1.0264
S37	8.29532	115.63542	0.2763	8.30087	115.64993	0.2435
Q38	8.33222	122.24746	0.1263	8.33179	122.25491	0.1201
A39	8.26324	125.18187	0.5204	8.27154	125.18082	0.5442
A39'	8.21669	124.52618	0.0033	8.216	124.498	0
M40	8.28335	119.4919	0.623	8.28331	119.48959	0.5674
D41	8.21269	121.03548	0.9643	8.2127	121.0334	0.9262
D41'	8.178	120.55	0	8.17773	120.5506	0.0046
D42	8.201	120.26399	1.6214	8.20098	120.26125	1.5793
D42'	8.16458	119.78222	0.0116	8.16529	119.77031	0.0103
L43	8.03609	121.71114	1.3089	8.03614	121.70784	1.2309
L43'	8.01294	121.44733	0.0088	8.01284	121.42484	0.0089
M44	8.21315	120.34038	0.5824	8.21488	120.2771	1.1817
L45	8.0384	123.14597	0.8651	8.04013	123.15377	0.8273
L45'	8.012	122.658	0	8.01262	122.66724	0.0089
S46	8.48319	118.43179	0.7947	8.49188	118.42941	0.7543
D48	8.17705	118.77493	0.8536	8.17703	118.76389	0.8203
D49	8.04803	120.17868	0.9748	8.04798	120.16766	0.9066
D49'	8.6017	119.78046	0.0121	8.05961	119.78034	0.0216
I50	7.80082	120.16756	1.266	7.80081	120.16464	1.1876
I50'	7.77034	119.78232	-0.0015	7.76586	119.87347	0.0096
E51	8.30138	123.65692	0.7759	8.3019	123.64158	0.8136
Q52	8.09497	120.36002	0.8503	8.0952	120.35741	0.8042
W53	7.93033	121.42083	1.4122	7.93033	121.4204	1.3398
F54	7.94005	121.51907	0.6229	7.93514	121.51455	0.9497
T55	7.94203	116.21425	0.4538	7.94207	116.21436	0.422
T55'	7.93027	116.00203	0.0581	7.92996	116.01849	0.0602
E56	8.25967	123.35468	0.7791	8.25973	123.34685	0.7574
E56'	8.25937	123.18397	-0.0158	8.26213	123.18198	-0.0304
D57	8.40081	123.39989	0.7176	8.40076	123.40179	0.7156
G59	8.36561	109.36705	0.9631	8.36556	109.36362	0.9858
D61	8.41259	119.87824	0.7463	8.41269	119.8772	0.7465
E62	8.07148	120.84271	0.846	8.07147	120.84074	0.8186
A63	8.23118	126.62881	0.906	8.23637	126.62611	0.9901
R65	8.4247	121.90302	0.9793	8.42445	121.90051	0.989
M66	8.43633	123.34866	0.4857	8.43632	123.34686	0.4758
E68	8.49507	121.22816	0.8099	8.506	121.22534	0.7699
A69	8.26368	125.38717	0.6735	8.26361	125.3966	0.5666
A70	8.18907	124.89296	0.9293	8.18925	124.89098	0.9914
R72	8.44038	122.48113	0.8507	8.44126	122.48224	0.7891
V73	7.70656	125.50375	1.1515	7.70678	125.49516	1.1029

	[.014mM]			[.024mM]		
Residue	H shift	N shift	Intensity	H shift	N shift	Intensity
M1	8.38923	121.6087	0.3546	8.38923	121.6087	0.3566
E2	8.3539	122.12215	0.6694	8.3539	122.12215	0.6741
E3	8.38911	123.54029	1.0928	8.38904	123.54163	1.0815
Q5	8.51855	121.03008	0.5572	8.51855	121.03008	0.5548
S6	8.34212	117.75113	0.2419	8.34212	117.75113	0.2479
D7	8.39852	123.68642	0.2149	8.39852	123.68642	0.2292
S9	8.4833	116.01527	0.502	8.4833	116.01527	0.5067
V10	7.82436	121.12621	0.7718	7.82436	121.12621	0.7551
E11	8.29506	126.14113	0.9605	8.29506	126.14113	0.9286
L14	8.30657	122.47572	0.8653	8.30657	122.47572	0.8452
S15	8.2833	116.69073	0.3542	8.2833	116.69073	0.3354
S15'	8.35059	116.87302	0.0086	8.35197	116.87196	0.0196
Q16	8.44406	122.55728	0.3025	8.44406	122.55728	0.3034
E17	8.42439	121.98997	0.4094	8.42439	121.98997	0.3969
T18	8.06457	114.89224	0.3336	8.06526	114.89112	0.3133
T18'	8.39235	113.99249	0.0021	8.3991	113.991	0.0143
F19	8.20066	122.28397	0.36	8.20066	122.28397	0.3426
F19'	8.14255	123.14256	-0.0084	8.14201	123.14322	0.0112
S20	8.0597	116.78655	0.1461	8.0599	116.7365	0.1428
S20'	7.94381	117.18866	-0.0053	7.94163	117.15009	0.0103
D21	8.23641	122.09476	0.2485	8.23641	122.09476	0.2431
D21'	8.11848	121.41582	0.1227	8.11845	121.41614	0.108
L22	7.90665	121.12763	0.9493	7.90665	121.12763	0.9194
W23	7.81257	119.39229	1.0032	7.81258	119.39198	0.9287
W23'	7.76012	119.39387	0.0071	7.76036	119.4002	-0.0011
K24	7.54213	120.45217	0.63	7.54738	120.45442	0.5661
K24'	7.30094	120.16608	0.0052	7.3009	120.15989	0.0014
L25	7.78892	120.74149	0.7503	7.78915	120.74128	0.7126
L25'	7.91	120.64184	-0.0002	7.90343	120.64144	0.0119
L26	7.87133	123.73	0.8873	7.87147	123.73123	0.825
E28	8.67176	119.7763	0.8301	8.67167	119.77691	0.8067
N29	8.23604	118.81183	0.3065	8.23623	118.81213	0.2791
N29'	8.23631	119.10083	0.0213	8.22622	119.00491	0.0189
N30	8.24799	119.58353	0.1936	8.24799	119.58353	0.1742
V31	7.98911	120.16245	0.7038	7.98911	120.16245	0.6527
D49'	8.05972	119.7767	0.0226	8.05605	119.77391	0.031
L32	8.24799	125.46648	0.7908	8.24799	125.46648	0.7496
S33	8.1773	118.04125	0.4597	8.1773	118.04125	0.4388
S33'	8.17725	118.33118	0.0262	8.16996	118.32503	0.0326
L35	8.25976	123.73082	1.0615	8.25976	123.73082	0.9872
S37	8.29497	115.62962	0.2593	8.29497	115.62962	0.2401
Q38	8.3309	122.22765	0.243	8.3309	122.22765	0.2131
A39	8.25993	125.17676	0.5382	8.25993	125.17676	0.4961
A39'	8.21228	124.50417	0.0071	8.20049	124.50532	0.0111
M40	8.2833	119.48781	0.5892	8.2833	119.48781	0.5398
D41	8.21256	121.03039	0.9224	8.21256	121.03039	0.8614
D41'	8.17725	120.548	0.0151	8.17736	120.54665	0.0277

	[.014mM]			[.024mM]		
Residue	H shift	N shift	Intensity	H shift	N shift	Intensity
D42	8.2008	120.26083	1.5598	8.20088	120.25868	1.4762
D42'	8.16556	119.77784	0.02237	8.16535	119.87924	0.04205
L43	8.03618	121.70514	1.2681	8.03618	121.70514	1.1931
L43'	8.01255	121.41573	0.0156	8.01252	121.41614	0.0264
M44	8.21408	120.31093	0.5017	8.20812	120.31508	0.4763
L45	8.03618	123.15159	0.8965	8.03627	123.1522	0.8257
L45'	8.01564	122.6698	0.0142	8.01554	122.66982	0.0257
S46	8.48325	118.42659	0.7791	8.48347	118.42639	0.7395
D48	8.17646	118.80756	0.7635	8.17328	118.77209	0.7292
D49	8.04798	120.16766	0.8684	8.04798	120.16766	0.8327
I50	7.80082	120.16286	1.24	7.80082	120.16286	1.1519
I50'	7.78904	119.77681	0.0427	7.77709	119.7031	0.0309
E51	8.2952	123.63458	0.9049	8.2952	123.63458	0.8489
Q52	8.09511	120.35492	0.8552	8.09511	120.35492	0.7781
W53	7.93032	121.41653	1.3399	7.93024	121.41675	1.2569
F54	7.93017	121.51328	0.941	7.9301	121.51237	0.8866
T55	7.94203	116.24724	0.4279	7.94203	116.24724	0.4119
T55'	7.9184	116.01701	0.053	7.9263	116.01154	0.062
E56	8.25976	123.34568	0.7502	8.25976	123.34568	0.7203
E56'	8.25952	123.05432	-0.0081	8.26033	123.05566	0.0064
D57	8.40071	123.44263	0.622	8.40105	123.44192	0.6388
G59	8.36579	109.36194	0.9321	8.36567	109.36174	0.9316
D61	8.41274	119.87355	0.6735	8.41274	119.87355	0.6826
E62	8.0715	120.83833	0.806	8.07143	120.83772	0.7837
A63	8.22443	126.62372	0.9329	8.22443	126.62372	0.9017
R65	8.42455	121.89954	0.9338	8.42455	121.89954	0.9265
M66	8.43616	123.34426	0.488	8.43623	123.3463	0.4845
E68	8.49502	121.22367	0.8319	8.49502	121.22367	0.8165
A69	8.25981	125.36871	0.636	8.25981	125.36871	0.6251
A70	8.18906	124.88745	0.8692	8.18907	124.88765	0.9121
R72	8.43628	122.47785	0.896	8.43628	122.47785	0.8756
V73	7.70668	125.56261	1.0975	7.70649	125.52828	1.1079

	[.045mM]			[.062mM]		
Residue	H shift	N shift	Intensity	H shift	N shift	Intensity
M1	8.38923	121.6087	0.3383	8.38923	121.6087	0.3413
E2	8.3539	122.12215	0.6496	8.3539	122.17342	0.6554
E3	8.38928	123.53702	1.0275	8.38928	123.53702	0.9401
Q5	8.51872	121.0308	0.5383	8.51872	121.0308	0.5264
S6	8.34212	117.75113	0.2395	8.34212	117.75113	0.2479
D7	8.401	123.69793	0.2365	8.4011	123.70457	0.2585
S9	8.48336	116.01526	0.4624	8.48336	116.01526	0.4544
V10	7.82436	121.12621	0.7349	7.82436	121.12621	0.7231

	[.045mM]			[.062mM]		
Residue	H shift	N shift	Intensity	H shift	N shift	Intensity
E11	8.29506	126.14113	0.8493	8.29506	126.14113	0.7461
L14	8.30687	122.47622	0.7709	8.30687	122.47622	0.6293
S15	8.2833	116.69073	0.2591	8.2833	116.69073	0.1596
S15'	8.3539	116.88183	0.0637	8.3553	116.87572	0.1206
Q16	8.44458	122.55947	0.2987	8.44481	122.55713	0.269
E17	8.42457	121.99548	0.3634	8.4221	121.99588	0.2908
T18	8.06526	114.89112	0.2313	8.06526	114.89112	0.1358
T18'	8.39528	113.56627	0.0223	8.39428	113.53852	0.0486
F19	8.20087	122.28477	0.2584	8.2011	122.28437	0.1523
F19'	8.14899	123.12342	0.0432	8.15382	123.15038	0.0947
S20	8.06758	116.7171	0.0793	8.05979	116.693	0.0598
S20'	7.94218	117.17709	0.0239	7.94705	117.17188	0.0664
D21	8.23639	122.09078	0.1941	8.23623	122.09129	0.1004
D21'	8.12137	121.38597	0.1279	8.11855	121.41592	0.1125
L22	7.90665	121.12763	0.7249	7.90665	121.12763	0.4233
W23	7.81258	119.39198	0.7134	7.81259	119.39117	0.3508
W23'	7.76006	119.39952	0.0109	7.76563	119.39127	0.0446
K24	7.55246	120.45177	0.4645	7.5494	120.4679	0.2337
K24'	7.30707	120.16049	0.0218	7.30701	120.16255	0.0327
L25	7.78915	120.74128	0.562	7.78915	120.74128	0.2876
L25'	7.90014	123.65062	0.0558	7.89981	120.64171	0.1151
L26	7.87147	123.73123	0.6108	7.87143	123.7297	0.3057
E28	8.67167	119.77691	0.6154	8.67167	119.77691	0.3183
N29	8.23613	118.8113	0.2434	8.23613	118.8113	0.1228
N29'	8.22493	119.00438	0.0657	8.22449	119.00461	0.1204
N30	8.24799	119.58353	0.1433	8.24799	119.58353	0.0845
V31	7.98911	120.16245	0.5204	8.0013	120.16348	0.3602
D49'	8.059464	119.77682	0.0678	8.05978	119.7765	0.1507
L32	8.24895	125.48112	0.6019	8.24895	125.48112	0.3673
S33	8.1773	118.04125	0.3402	8.1773	118.04125	0.1905
S33'	8.16221	118.33614	0.0931	8.16548	118.32985	0.1815
L35	8.25976	123.73082	0.7644	8.25976	123.73082	0.4128
S37	8.29506	115.62952	0.1986	8.29634	115.64872	0.1104
Q38	8.33322	122.22303	0.1712	8.33511	122.21838	0.1219
A39	8.25993	125.17676	0.3866	8.25993	125.17676	0.2121
A39'	8.2011	124.50149	0.0414	8.20127	124.5013	0.0943
M40	8.2833	119.48781	0.446	8.2833	119.48781	0.2448
D41	8.21256	121.03039	0.677	8.21256	121.03039	0.3797
D41'	8.17715	120.54726	0.0822	8.17741	120.5484	0.1753
D42	8.20088	120.25868	1.1786	8.20088	120.25868	0.6583
D42'	8.16574	119.8742	0.0964	8.16562	119.87294	0.2362
L43	8.03618	121.70514	0.9265	8.03618	121.70514	0.5193
L43'	8.01262	121.41447	0.1093	8.01264	121.41512	0.1829
M44	8.20812	120.31508	0.3913	8.20623	120.30077	0.6583

	[.045mM]			[.062mM]		
Residue	H shift	N shift	Intensity	H shift	N shift	Intensity
L45	8.0362	123.15106	0.6353	8.0362	123.15106	0.345
L45'	8.01254	122.67055	0.0837	8.01257	122.66941	0.1713
S46	8.48337	118.4266	0.5812	8.48926	118.42598	0.3476
D48	8.17328	118.77209	0.5808	8.17328	118.77209	0.3276
D49	8.04804	120.16246	0.6966	8.04804	120.16246	0.422
I50	7.80085	120.16204	0.9048	7.80085	120.16204	0.4973
I50'	7.77729	119.96959	0.0967	7.77748	119.96928	0.1917
E51	8.2952	123.63458	0.6853	8.2952	123.63458	0.3921
Q52	8.09511	120.35492	0.6067	8.09511	120.35492	0.3288
W53	7.93024	121.41675	1.0157	7.93024	121.41675	0.5784
F54	7.93023	121.51081	0.696	7.93023	121.51081	0.4011
T55	7.94203	116.24724	0.3394	7.94203	116.24724	0.2116
T55'	7.93024	115.91903	0.0754	7.93024	115.92741	0.1649
E56	8.25976	123.34568	0.6282	8.26578	123.3463	0.4614
E56'	8.26315	123.05515	0.06254	8.25975	123.05536	0.1442
D57	8.4008	123.38837	0.4484	8.4008	123.38837	0.4033
G59	8.36567	109.36174	0.8899	8.36567	109.36174	0.8146
D61	8.41274	119.87355	0.6392	8.41272	119.96835	0.6308
E62	8.07143	120.83772	0.7549	8.07143	120.83772	0.6781
A63	8.22443	126.62372	0.8537	8.22944	126.62392	0.8118
R65	8.4243	121.89832	0.8791	8.4243	121.89832	0.7645
M66	8.43623	123.34435	0.4777	8.43629	123.34487	0.4494
E68	8.49507	121.22337	0.7763	8.49507	121.22337	0.7415
A69	8.25976	125.37285	0.6231	8.25994	125.36953	0.6243
A70	8.18907	124.88765	0.9218	8.18907	124.88765	0.9243
R72	8.43628	122.47785	0.8535	8.43618	122.47694	0.8209
V73	7.70653	125.47323	1.1202	7.70649	125.46668	1.151

	[.076mM]			[.101mM]		
Residue	H shift	N shift	Intensity	H shift	N shift	Intensity
M1	8.38923	121.6087	0.308	8.38923	121.6087	0.2943
E2	8.3539	122.17342	0.6211	8.35395	122.18784	0.5946
E3	8.38928	123.53702	0.8422	8.38928	123.53702	0.7884
Q5	8.51863	121.02977	0.4995	8.51863	121.02977	0.4861
S6	8.34212	117.75113	0.2519	8.34212	117.75113	0.2396
D7	8.40089	123.70753	0.2799	8.40071	123.71452	0.2867
S9	8.49508	116.01547	0.4573	8.49508	116.01547	0.4516
V10	7.82436	121.12621	0.6827	7.82436	121.12621	0.6719
E11	8.30128	126.14583	0.6503	8.30164	126.16378	0.5864
L14	8.30687	122.47622	0.5352	8.31492	122.50206	0.5685
S15	8.28909	116.69427	0.086	8.28896	116.69362	0.0331
S15'	8.35394	116.88371	0.1515	8.35398	116.88361	0.2129
Q16	8.44481	122.55713	0.2576	8.44481	122.55713	0.2343

	[.076mM]			[.101mM]		
Residue	H shift	N shift	Intensity	H shift	N shift	Intensity
E17	8.40696	122.04971	0.1127	8.40696	122.04971	0.1415
T18	8.06986	114.86888	0.0716	8.06235	114.86573	0.0168
T18'	8.39284	113.53625	0.0604	8.39692	113.57674	0.072
F19	8.20181	122.28648	0.0881	8.20609	122.28827	0.0202
F19'	8.15383	123.15179	0.1249	8.15384	123.15159	0.1599
S20	8.07108	116.69465	0.0351	8.07269	116.69218	0.0092
S20'	7.94629	117.1763	0.0766	7.94226	117.17665	0.1058
D21	8.23581	122.17249	0.1076	8.23581	122.17249	0.0518
D21'	8.12176	121.39339	0.1076	8.11889	121.40819	0.1102
L22	7.91451	121.1258	0.2696	7.91846	121.1291	0.2696
W23	7.81259	119.39117	0.161	7.81211	119.38329	0.0366
W23'	7.76565	119.39127	0.0594	7.76504	119.38757	0.0904
K24	7.5494	120.4679	0.1161	7.55353	120.43309	0.0439
K24'	7.31795	120.160.11	0.0332	7.31831	120.16344	0.0439
L25	7.78915	120.74128	0.1291	7.78895	120.74191	0.0175
L25'	7.90666	120.64413	0.1369	7.90099	120.64444	0.1817
L26	7.87143	123.7297	0.1302	7.87196	123.73206	0.0705
E28	8.67167	119.77691	0.1499	8.67167	119.77691	0.0247
N29	8.23608	118.81619	0.0723	8.23574	118.81131	0.0225
N29'	8.2246	119.00409	0.1526	8.22463	119.00521	0.1833
N30	8.24671	119.58115	0.0488	8.24799	119.58353	0.0186
V31	8.00073	120.15081	0.2733	8.01266	120.10526	0.3242
D49'	8.05969	119.7766	0.1844	8.05972	119.7763	0.2248
L32	8.24895	125.48112	0.2203	8.23262	125.72092	0.0589
S33	8.17739	118.04185	0.1085	8.17735	118.04178	0.0325
S33'	8.16562	118.33086	0.2406	8.1596	118.33817	0.2822
L35	8.25976	123.73082	0.2156	8.27118	123.63547	0.0796
S37	8.26847	115.31998	0.0613	8.26847	115.31998	0.0789
Q38	8.33511	122.21838	0.0853	8.31953	122.27681	0.0828
A39	8.26364	125.18227	0.1092	8.34804	124.90046	0.0569
A39'	8.20092	124.50201	0.1107	8.20095	124.50397	0.1472
M40	8.2833	119.48781	0.1413	8.2833	119.48781	0.0483
D41	8.21271	121.03008	0.2012	8.21256	121.02966	0.0615
D41'	8.17734	120.5481	0.2132	8.17729	120.54769	0.2705
D42	8.20088	120.25868	0.3729	8.20136	120.25745	0.1218
D42'	8.16561	119.87254	0.2863	8.16562	119.87273	0.3853
L43	8.03618	121.70514	0.2919	8.03618	121.70514	0.09
L43'	8.01881	121.41532	0.2335	8.01254	121.41469	0.3172
M44	8.20247	120.29118	0.3729	8.20092	120.25786	0.1218
L45	8.03664	123.11062	0.1826	8.03645	123.06091	0.0647
L45'	8.01265	122.6695	0.216	8.0142	122.66264	0.2777
S46	8.49516	118.42599	0.2568	8.51188	118.37444	0.2368
D48	8.17521	118.71805	0.2095	8.16567	118.7159	0.1014
D49	8.04804	120.16246	0.2809	8.04804	120.16246	0.1203

	[.076mM]			[.101mM]		
Residue	H shift	N shift	Intensity	H shift	N shift	Intensity
I50	7.80085	120.16204	0.2796	7.80111	120.16142	0.0921
I50'	7.7773	119.96928	0.2269	7.77738	119.96917	0.3187
E51	8.2952	123.63458	0.2323	8.2952	123.63458	0.0761
Q52	8.09511	120.35492	0.1711	8.09501	120.35492	0.0429
W53	7.93034	121.41593	0.3402	7.92757	121.38475	0.1194
F54	7.93055	121.4903	0.2269	7.93004	121.45496	0.1194
T55	7.942	116.20773	0.1349	7.94187	116.20855	0.0487
T55'	7.93029	115.91792	0.1936	7.92987	115.92278	0.2348
E56	8.27169	123.34507	0.4727	8.27169	123.34507	0.494
E56'	8.25975	123.05515	0.1821	8.25976	123.05556	0.2402
D57	8.40072	123.39043	0.3724	8.40088	123.39236	0.3369
G59	8.36567	109.36174	0.7611	8.36567	109.36174	0.7011
D61	8.41273	119.96958	0.6562	8.41272	119.96835	0.6671
E62	8.07143	120.83772	0.6066	8.07169	120.8383	0.5764
A63	8.23618	126.62352	0.8927	8.23618	126.62352	0.8654
R65	8.4243	121.89832	0.7018	8.42088	121.89812	0.6173
M66	8.43629	123.34487	0.4246	8.4363	123.34363	0.4056
E68	8.50083	121.22356	0.6751	8.50083	121.22356	0.6841
A69	8.25994	125.36953	0.5876	8.25994	125.36953	0.5668
A70	8.18907	124.88765	0.9097	8.18907	124.88765	0.8827
R72	8.43618	122.47694	0.7724	8.43618	122.47694	0.7598
V73	8.1742012	121.32843	1.1754	7.70649	125.46668	1.1921

	[.133mM]			[.165mM]		
Residue	H shift	N shift	Intensity	H shift	N shift	Intensity
M1	8.38917	121.60741	0.28	8.38928	121.60867	0.272
E2	8.35383	122.18665	0.541	8.35383	122.18665	0.5635
E3	8.38928	123.53702	0.7538	8.39451	123.53779	0.6762
Q5	8.51859	121.02879	0.4913	8.5303	121.03094	0.4878
S6	8.34206	117.75025	0.2328	8.34228	117.75196	0.2322
D7	8.40125	123.71524	0.2945	8.40088	123.63309	0.2916
S9	8.49498	116.01407	0.416	8.49512	116.0164	0.464
V10	7.82436	121.12621	0.6593	7.82436	121.12621	0.6358
E11	8.29983	126.16666	0.5985	8.30659	126.21333	0.628
L14	8.31842	122.50247	0.5424	8.31862	122.57189	0.6664
S15	8.28896	116.69362	0.0128	8.28896	116.69362	0.0078
S15'	8.35386	116.88273	0.2485	8.35395	116.88362	0.28
Q16	8.47139	122.57313	0.1464	8.47628	122.57929	0.1588
E17	8.4014	122.04575	0.1953	8.4014	122.04575	0.2146
T18	8.06195	114.79726	0.0006	8.06077	114.7972	-0.0031
T18'	8.39063	113.51651	0.0788	8.39463	113.55564	0.0815
F19	8.19927	122.28517	0.0121	8.20932	122.28302	0.007
F19'	8.15384	123.15159	0.1761	8.15384	123.15159	0.1926
S20	8.07205	116.68913	-0.0075	8.07419	116.68092	0.0085
S20'	7.94206	117.17443	0.1024	7.94208	117.17291	0.1059

	[.133mM]			[.165mM]		
Residue	H shift	N shift	Intensity	H shift	N shift	Intensity
D21	8.22463	122.08878	0.0127	8.2168	122.00046	0.00396
D21'	8.11854	121.41432	0.1172	8.11854	121.41432	0.0995
L22	7.91846	121.1291	0.2878	7.91846	121.1291	0.307
W23	7.81407	119.39039	0.0144	7.81316	119.9313	0.04218
W23'	7.76504	119.38757	0.0887	7.76504	119.38757	0.0966
K24	7.55046	120.45242	0.0023	7.55927	120.45548	-0.0003
K24'	7.30677	120.16496	0.0548	7.30571	120.15898	0.055
L25	7.78895	120.74191	-0.0055	7.78895	120.74191	0.0051
L25'	7.89491	120.64241	0.2046	7.89501	120.54768	0.1892
L26	7.87196	123.73206	0.0101	7.87196	123.73206	0.003
E28	8.67167	119.77691	0.0003	8.67167	119.77691	0.0108
N29	8.23613	118.81179	0.0152	8.23649	118.8059	0.0224
N29'	8.22419	118.99843	0.2106	8.22425	119.00497	0.2128
N30	8.24799	119.58353	0.0013	8.24799	119.58353	0.004
V31	8.01266	120.10526	0.3583	8.01267	120.06514	0.3794
D49'	8.05967	119.77511	0.2532	8.05916	119.70339	0.2227
L32	8.23262	125.72092	0.0376	8.23262	125.72092	0.0503
S33	8.17735	118.04178	0.009	8.17735	118.04178	0.0074
S33'	8.15378	118.32928	0.3281	8.15378	118.32928	0.3208
L35	8.27118	123.63547	0.0353	8.27118	123.63547	0.0403
S37	8.25967	115.33901	0.1058	8.25977	115.34061	0.1016
Q38	8.31953	122.27681	0.0795	8.31953	122.27681	0.0798
A39	8.34804	124.90046	0.0558	8.34804	124.90046	0.0659
A39'	8.20096	124.50009	0.1767	8.20117	124.50153	0.1791
M40	8.2833	119.48781	0.0209	8.2833	119.48781	0.0146
D41	8.21256	121.02966	0.026	8.21256	121.02966	0.0291
D41'	8.17729	120.54769	0.2878	8.17729	120.54769	0.3104
D42	8.20136	120.25745	0.0685	8.20136	120.25745	0.0395
D42'	8.16556	119.87133	0.4335	8.16556	119.87133	0.4513
L43	8.03618	121.70514	0.0475	8.03618	121.70514	0.018
L43'	8.01276	121.41432	0.3712	8.01276	121.41432	0.3238
M44	8.20092	120.25786	0.0685	8.20092	120.25786	0.0395
L45	8.0356	123.05416	0.0334	8.02417	123.05588	0.0195
L45'	8.01233	122.66862	0.3205	8.01285	122.66582	0.2933
S46	8.51201	118.32928	0.2609	8.51874	118.33	0.2714
D48	8.16545	118.7165	0.0547	8.16545	118.7165	0.0462
D49	8.04804	120.16246	0.0574	8.04804	120.16246	0.0508
I50	7.80111	120.16142	0.0538	7.80111	120.16142	0.0262
I50'	7.77738	119.96917	0.3384	7.77738	119.96917	0.3331
E51	8.2952	123.63458	0.0438	8.2952	123.63458	0.0222
Q52	8.09501	120.35492	0.0242	8.09501	120.35492	-0.0024
W53	7.92757	121.38475	0.0639	7.92757	121.38475	0.0279
F54	7.93004	121.45496	0.0639	7.93004	121.45496	0.0279
T55	7.94187	116.20855	0.022	7.94187	116.20855	0.0095
T55'	7.9302	115.91638	0.2518	7.93061	115.87907	0.2057
E56	8.27141	123.34421	0.4804	8.27141	123.34421	0.4392
E56'	8.25974	123.05584	0.2915	8.25974	123.05584	0.2764

	[.133mM]			[.165mM]		
Residue	H shift	N shift	Intensity	H shift	N shift	Intensity
D57	8.40062	123.39305	0.4768	8.40062	123.39305	0.4622
G59	8.36567	109.36174	0.648	8.36567	109.36305	0.6548
D61	8.41272	119.96835	0.6579	8.41272	119.96835	0.6776
E62	8.07165	120.83633	0.5683	8.083	120.83665	0.607
A63	8.23618	126.62352	0.7958	8.23641	126.62217	0.8848
R65	8.41266	121.89671	0.6154	8.41266	121.89671	0.5588
M66	8.4363	123.34363	0.392	8.4363	123.34363	0.3956
E68	8.49557	121.22229	0.6822	8.5073	121.22255	0.6826
A69	8.25989	125.36803	0.5732	8.25991	125.36946	0.5303
A70	8.18921	124.88626	0.8411	8.18921	124.88626	0.8929
R72	8.43612	122.47555	0.7693	8.44099	122.47629	0.7279
V73	7.70663	125.46456	1.1486	7.70671	125.46506	1.2444

	[.198mM]			[.222mM]		
Residue	H shift	N shift	Intensity	H shift	N shift	Intensity
M1	8.38938	121.60709	0.2956	8.38922	121.6091	0.2982
E2	8.35383	122.18665	0.5586	8.354	122.1863	0.5945
E3	8.39451	123.53779	0.7754	8.39451	123.53779	0.7373
Q5	8.51898	121.03033	0.5146	8.52444	121.02947	0.4519
S6	8.34217	117.75014	0.2325	8.34217	117.75014	0.2312
D7	8.3893	123.63197	0.2778	8.40077	123.63408	0.2792
S9	8.48867	116.01438	0.4199	8.49523	116.01608	0.4386
V10	7.82436	121.12621	0.6628	7.82436	121.12621	0.6464
E11	8.29505	126.21198	0.6232	8.30084	126.19936	0.558
L14	8.31862	122.57189	0.6275	8.31855	122.57297	0.6612
S15	8.28896	116.69362	0.0038	8.28896	116.69362	0.0097
S15'	8.35388	116.8818	0.2778	8.35394	116.88401	0.2784
Q16	8.47143	122.60232	0.1369	8.47143	122.60232	0.1388
E17	8.40096	121.99223	0.2593	8.40102	122.05013	0.2112
T18	8.05978	114.79765	-0.0082	8.05889	114.79629	-0.0026
T18'	8.3887	113.55099	0.089	8.38893	113.60092	0.084
F19	8.21387	122.28477	0.0032	8.21418	122.28189	0.0062
F19'	8.15386	123.1506	0.1922	8.15386	123.1506	0.202
S20	8.07183	116.68294	-0.0068	8.07116	116.6813	-0.0011
S20'	7.94209	117.1761	0.1152	7.94637	117.17074	0.1184
D21	8.22433	122.08356	0.0109	8.22405	122.03922	0.0036
D21'	8.11854	121.41432	0.1155	8.11867	121.41603	0.1161
L22	7.91853	121.12543	0.2703	7.91853	121.12543	0.235
W23	7.81048	119.39139	0.0419	7.81078	119.38993	0.0171
W23'	7.76504	119.38757	0.1081	7.76504	119.38757	0.0996
K24	7.54996	120.45016	-0.0042	7.55023	120.45084	-0.0071
K24'	7.30631	120.16086	0.0495	7.30656	120.16401	0.0547
L25	7.78895	120.74191	0.0017	7.78895	120.74191	-0.0032
L25'	7.89506	120.54639	0.1789	7.89493	120.45217	0.1707
L26	7.87196	123.73206	-0.0038	7.87196	123.73206	-0.0029

	[.198mM]			[.222mM]		
Residue	H shift	N shift	Intensity	H shift	N shift	Intensity
E28	8.67167	119.77691	-0.0078	8.67167	119.77691	-0.0006
N29	8.23619	118.80508	0.0195	8.23639	118.80426	0.031
N29'	8.22427	118.90582	0.1801	8.22464	118.90681	0.21
N30	8.24799	119.58353	-0.0026	8.24799	119.58353	0.0071
V31	8.00096	120.06462	0.3995	8.00084	120.06561	0.3731
D49'	8.04805	119.67847	0.2286	8.04791	119.67956	0.2077
L32	8.23262	125.72092	0.0312	8.23262	125.72092	0.0362
S33	8.17735	118.04178	0.0202	8.17735	118.04178	0.0044
S33'	8.15378	118.32928	0.3308	8.15368	118.32975	0.3171
L35	8.27118	123.63547	0.0348	8.27118	123.63547	0.0314
S37	8.25977	115.3386	0.1034	8.25977	115.3386	0.0996
Q38	8.31953	122.27681	0.0804	8.31953	122.27681	0.0784
A39	8.34804	124.90046	0.0557	8.34804	124.90046	0.0611
A39'	8.20096	124.50072	0.1969	8.20096	124.50072	0.1774
M40	8.2833	119.48781	-0.0017	8.2833	119.48781	0.0051
D41	8.21256	121.02966	0.0174	8.21256	121.02966	0.0086
D41'	8.17287	120.5546	0.2655	8.17481	120.59373	0.2622
D42	8.20136	120.25745	0.0118	8.20136	120.25745	0.0152
D42'	8.16556	119.87133	0.4152	8.16551	119.87253	0.4352
L43	8.03618	121.70514	0.0139	8.03618	121.70514	0.0042
L43'	8.01258	121.31799	0.3297	8.01269	121.3201	0.3209
M44	8.20092	120.25786	0.0118	8.20092	120.25786	0.0152
L45	8.02413	123.05511	0.0074	8.02434	123.05535	-0.0004
L45'	8.00076	122.57062	0.2518	8.00102	122.57317	0.2619
S46	8.50693	118.32876	0.251	8.51182	118.32975	0.247
D48	8.16545	118.7165	0.0306	8.16545	118.7165	0.0137
D49	8.04804	120.16246	0.0222	8.04804	120.16246	0.0099
I50	7.80111	120.16142	0.0203	7.80111	120.16142	0.0133
I50'	7.76545	119.96829	0.3402	7.7656	119.97009	0.3161
E51	8.2952	123.63458	0.0184	8.2952	123.63458	0.017
Q52	8.09501	120.35492	-0.0069	8.09501	120.35492	0.0008
W53	7.92757	121.38475	0.0194	7.92757	121.38475	0.009
F54	7.93004	121.45496	0.0194	7.93004	121.45496	0.009
T55	7.94187	116.20855	0.0001	7.94187	116.20855	0.0061
T55'	7.91853	115.82202	0.2309	7.91855	115.78225	0.1936
E56	8.27141	123.34421	0.4374	8.27168	123.34446	0.421
E56'	8.25965	122.95834	0.2385	8.25445	122.9575	0.2153
D57	8.39559	123.39256	0.3867	8.3956	123.39436	0.3647
G59	8.36567	109.36305	0.5681	8.36562	109.36112	0.5675
D61	8.41272	119.96835	0.6551	8.41269	119.96917	0.6681
E62	8.07796	120.83571	0.5511	8.0832	120.8371	0.6072
A63	8.22788	126.62232	0.786	8.23626	126.62331	0.8262
R65	8.41266	121.89671	0.6162	8.41928	121.89771	0.5716
M66	8.4363	123.34363	0.3832	8.4363	123.34363	0.37
E68	8.49492	121.22258	0.7059	8.50517	121.22458	0.65
A69	8.25965	125.36824	0.5772	8.25961	125.37004	0.5265

	[.198mM]			[.222mM]		
Residue	H shift	N shift	Intensity	H shift	N shift	Intensity
A70	8.18921	124.88626	0.8264	8.18907	124.88734	0.8678
R72	8.43637	122.47503	0.7756	8.43645	122.47694	0.7223
V73	7.70671	125.46506	1.174	7.70674	125.46688	1.219

	[.237mm]			[.255mM]		
Residue	H shift	N shift	Intensity	H shift	N shift	Intensity
M1	8.39349	121.60856	0.2868	8.38948	121.60809	0.302
E2	8.354	122.1863	0.5909	8.354	122.1863	0.6031
E3	8.39869	123.52998	0.7773	8.39869	123.52998	0.7193
Q5	8.53011	121.03169	0.4826	8.52412	121.02864	0.472
S6	8.34217	117.75014	0.2352	8.34214	117.75123	0.2343
D7	8.40077	123.63538	0.2606	8.40097	123.63418	0.2657
S9	8.49514	116.01718	0.4668	8.49503	116.01578	0.4429
V10	7.82447	121.12762	0.6178	7.82432	121.12682	0.6462
E11	8.30644	126.2039	0.6349	8.30132	126.1895	0.561
L14	8.31855	122.57297	0.6862	8.31855	122.57297	0.668
S15	8.28896	116.69362	0.0122	8.28896	116.69362	0.009
S15'	8.3539	116.88491	0.2682	8.35386	116.88319	0.2829
Q16	8.47575	122.60954	0.1315	8.47383	122.61221	0.1395
E17	8.40102	122.05013	0.2061	8.40102	122.05013	0.1987
T18	8.0582	114.79623	0.0081	8.05575	114.79776	-0.0022
T18'	8.39511	113.55861	0.085	8.39074	113.50623	0.0892
F19	8.21386	122.28146	-0.0042	8.21347	122.28084	0.0033
F19'	8.15386	123.1506	0.2043	8.15374	123.15138	0.213
S20	8.07093	116.68061	0.0056	8.07049	116.68124	0.0036
S20'	7.95363	117.17339	0.1209	7.94623	117.1729	0.1174
D21	8.22426	122.00465	0.10192	8.22057	122.20609	0.0083
D21'	8.11867	121.41603	0.0961	8.11867	121.41603	0.1074
L22	7.91856	121.12762	0.238	7.90685	121.1092	0.2014
W23	7.814	119.39948	0.0184	7.80995	119.39005	0.009
W23'	7.76504	119.38757	0.099	7.76504	119.38757	0.1031
K24	7.54981	120.4541	0.0004	7.55501	120.45513	-0.0089
K24'	7.30647	120.16201	0.0601	7.30663	120.16286	0.0574
L25	7.78895	120.74191	-0.0055	7.78895	120.74191	-0.0083
L25'	7.89508	120.45266	0.1769	7.88929	120.41077	0.1367
L26	7.87196	123.73206	-0.0078	7.87196	123.73206	0.0041
E28	8.67167	119.77691	0.0012	8.67167	119.77691	0
N29	8.23634	118.80376	0.0438	8.23625	118.80348	0.0404
N29'	8.22396	118.91122	0.2088	8.22481	118.90748	0.2084
N30	8.24799	119.58353	0.0006	8.24799	119.58353	0.0089
V31	8.0006	120.06763	0.3727	8.0006	120.06763	0.3343
D49'	8.04762	119.68085	0.204	8.04769	119.58343	0.1901
L32	8.23262	125.72092	0.044	8.23262	125.72092	0.0452
S33	8.17735	118.04178	0.017	8.17735	118.04178	0.0044
S33'	8.154	118.33074	0.3019	8.15386	118.33015	0.2927

	[.237mm]			[.255mM]		
Residue	H shift	N shift	Intensity	H shift	N shift	Intensity
L35	8.27118	123.63547	0.0291	8.27118	123.63547	0.0266
S37	8.25977	115.3386	0.0903	8.25975	115.34061	0.1088
Q38	8.31953	122.27681	0.0757	8.31953	122.27681	0.0757
A39	8.34804	124.90046	0.0697	8.34804	124.90046	0.0668
A39'	8.20648	124.47939	0.1687	8.20084	124.47588	0.1767
M40	8.2833	119.48781	-0.0007	8.2833	119.48781	0.0007
D41	8.21256	121.02966	-0.0005	8.21256	121.02966	0.0055
D41'	8.17741	120.59417	0.2733	8.17214	120.59985	0.2619
D42	8.20136	120.25745	0.0095	8.20136	120.25745	0.0114
D42'	8.16567	119.8727	0.4458	8.16567	119.8727	0.4207
L43	8.03618	121.70514	0.0073	8.03618	121.70514	0.0017
L43'	8.0126	121.32101	0.3374	8.00105	121.31683	0.3018
M44	8.20092	120.25786	0.0095	8.20092	120.25786	0.0114
L45	8.02416	123.05584	0.0036	8.02398	123.05484	0.0143
L45'	8.00098	122.57417	0.2597	8.00067	122.57255	0.279
S46	8.51867	118.33136	0.2457	8.50697	118.33067	0.237
D48	8.16545	118.7165	0.0222	8.16545	118.7165	0.0157
D49	8.04804	120.16246	0.0115	8.04804	120.16246	0.0012
I50	7.80111	120.16142	0.0115	7.80111	120.16142	0.0003
I50'	7.7656	119.97009	0.3059	7.7656	119.97009	0.2724
E51	8.2952	123.63458	0.0181	8.2952	123.63458	0.0213
Q52	8.09501	120.35492	-0.0042	8.09501	120.35492	0.0006
W53	7.92757	121.38475	0.0084	7.92757	121.38475	0.0038
F54	7.93004	121.45496	0.0084	7.93004	121.45496	0.0038
T55	7.94187	116.20855	0.008	7.94187	116.20855	0.0094
T55'	7.91848	115.77831	0.1846	7.91383	115.72585	0.1909
E56	8.27151	123.34659	0.4071	8.2716	123.34435	0.4029
E56'	8.25972	122.96043	0.2108	8.24796	122.86197	0.229
D57	8.40092	123.3928	0.2993	8.39611	123.3956	0.3475
G59	8.36565	109.36211	0.5918	8.36565	109.36211	0.5457
D61	8.41286	119.97068	0.6757	8.41286	119.97068	0.6716
E62	8.08334	120.83799	0.6277	8.08334	120.83799	0.6084
A63	8.23626	126.62331	0.8962	8.23626	126.62331	0.8171
R65	8.42491	121.89787	0.6066	8.41786	121.89555	0.5745
M66	8.43968	123.3076	0.3537	8.43631	123.29803	0.3769
E68	8.50699	121.2254	0.7138	8.50699	121.2254	0.6606
A69	8.27009	125.37238	0.5303	8.2598	125.37004	0.5425
A70	8.18907	124.88734	0.8842	8.18907	124.88734	0.8648
R72	8.44147	122.47649	0.6763	8.44147	122.47649	0.7294
V73	7.70674	125.46688	1.2643	7.70672	125.46607	1.2303

	[.276mM]			[.285mM]		
Residue	H shift	N shift	Intensity	H shift	N shift	Intensity
M1	8.38923	121.6089	0.3128	8.38923	121.6089	0.3049
E2	8.35403	122.18784	0.6124	8.35403	122.18784	0.621

	[.276mM]			[.285mM]		
Residue	H shift	N shift	Intensity	H shift	N shift	Intensity
E3	8.39511	123.51105	0.7195	8.39511	123.51105	0.7196
Q5	8.52412	121.02864	0.4674	8.52412	121.02864	0.4619
S6	8.34214	117.75123	0.2261	8.34214	117.75123	0.2314
D7	8.40097	123.63418	0.2611	8.40097	123.63418	0.2647
S9	8.49503	116.01578	0.4429	8.49503	116.01578	0.4358
V10	7.82432	121.12682	0.6426	7.82432	121.12682	0.6355
E11	8.30132	126.1895	0.5495	8.30132	126.1895	0.5533
L14	8.31855	122.57297	0.674	8.31855	122.57297	0.6655
S15	8.28896	116.69362	-0.0003	8.28896	116.69362	0.003
S15'	8.35386	116.88319	0.2763	8.35386	116.88319	0.2904
Q16	8.4716	122.57481	0.1457	8.4716	122.57481	0.1405
E17	8.40102	122.05013	0.2038	8.40102	122.05013	0.2044
T18	8.05549	114.7958	0.0015	8.0552	114.79618	-0.0004
T18'	8.39173	113.6437	0.0958	8.38966	113.5078	0.0927
F19	8.21261	122.27972	-0.0072	8.21235	122.1261	0.0029
F19'	8.15384	123.15159	0.2005	8.15385	123.1517	0.2122
S20	8.07044	116.67995	0.0081	8.06574	116.67986	-0.0014
S20'	7.94265	117.17271	0.1251	7.94698	117.17292	0.109
D21	8.22549	122.00482	0.0002	8.21279	121.99455	0.0082
D21'	8.11858	121.41603	0.1058	8.11858	121.41603	0.1163
L22	7.90668	121.03059	0.1968	7.90668	121.03059	0.1956
W23	7.80993	119.38953	0.0143	7.81006	119.39179	0.0154
W23'	7.76572	119.39085	0.104	7.76548	119.39075	0.1023
K24	7.55	120.45279	0.0033	7.55128	120.45094	-0.0029
K24'	7.30583	120.16071	0.0574	7.30626	123.16391	0.0582
L25	7.78895	120.74191	0.0032	7.78895	120.74191	0.0054
L25'	7.88319	120.35502	0.1403	7.88316	120.35532	0.1498
L26	7.87196	123.73206	0.0048	7.87196	123.73206	0.0016
E28	8.67167	119.77691	0.0056	8.67167	119.77691	-0.0002
N29	8.23571	118.80332	0.0485	8.23509	118.80312	0.0561
N29'	8.21864	118.90712	0.1179	8.21282	118.90836	0.1769
N30	8.24799	119.58353	-0.0067	8.24799	119.58353	0.0044
V31	7.99621	120.05293	0.2772	7.99409	120.0436	0.2549
D49'	8.04097	119.58373	0.1651	8.03614	119.58312	0.1701
L32	8.23262	125.72092	0.0434	8.23262	125.72092	0.0425
S33	8.17735	118.04178	0.0079	8.17735	118.04178	0.003
S33'	8.15386	118.33015	0.2684	8.15383	118.32117	0.2657
L35	8.27118	123.63547	0.0276	8.27118	123.63547	0.0192
S37	8.25975	115.34061	0.1074	8.25975	115.34061	0.0952
Q38	8.31953	122.27681	0.0798	8.31953	122.27681	0.0849
A39	8.34804	124.90046	0.0596	8.34804	124.90046	0.0629
A39'	8.20093	124.47624	0.1739	8.20092	124.43839	0.1775
M40	8.2833	119.48781	0.0012	8.2833	119.48781	0.0064
D41	8.21256	121.02966	0.0024	8.21256	121.02966	0.0098
D41'	8.1686	120.60496	0.2779	8.16816	120.61414	0.2952
D42	8.20136	120.25745	0.0121	8.20136	120.25745	0.0058

	[.276mM]			[.285mM]		
Residue	H shift	N shift	Intensity	H shift	N shift	Intensity
D42'	8.16558	119.87181	0.4138	8.16556	119.87314	0.3891
L43	8.03618	121.70514	0.0006	8.03618	121.70514	0.005
L43'	8.00084	121.32011	0.2849	8.00084	121.32011	0.2621
M44	8.20092	120.25786	0.0121	8.20092	120.25786	0.0058
L45	8.02318	123.05349	0.0024	8.02328	122.04318	0.0046
L45'	8.00105	122.57224	0.02639	8.00073	122.56779	0.2372
S46	8.50685	118.33015	0.2045	8.50685	118.33015	0.2058
D48	8.16545	118.7165	0.0177	8.16545	118.7165	0.0147
D49	8.04804	120.16246	0.0045	8.04804	120.16246	-0.0022
I50	7.80111	120.16142	-0.0046	7.80111	120.16142	-0.001
I50'	7.7656	119.97009	0.249	7.7656	119.97009	0.2203
E51	8.2952	123.63458	0.0163	8.2952	123.63458	0.0125
Q52	8.09501	120.35492	-0.0012	8.09501	120.35492	-0.0048
W53	7.92757	121.38475	0.0029	7.92757	121.38475	0.0061
F54	7.93004	121.45496	0.0029	7.93004	121.45496	0.0061
T55	7.94187	116.20855	0.0073	7.94187	116.20855	0.0049
T55'	7.9067	115.72595	0.1762	7.90689	115.64133	0.1594
E56	8.2716	123.34435	0.3775	8.2716	123.34435	0.3687
E56'	8.24806	122.86309	0.2206	8.24806	122.86309	0.1952
D57	8.39202	123.38915	0.2804	8.39443	123.38213	0.2826
G59	8.36547	109.33525	0.5157	8.36547	109.33525	0.4982
D61	8.41276	119.96958	0.6818	8.41276	119.96958	0.665
E62	8.08322	120.8369	0.6043	8.08322	120.8369	0.6026
A63	8.23643	126.62383	0.7974	8.23609	126.62372	0.7887
R65	8.41815	121.89729	0.563	8.41815	121.89729	0.5641
M66	8.43628	123.32943	0.3696	8.43628	123.32943	0.3694
E68	8.5067	121.22204	0.6529	8.5067	121.22204	0.6466
A69	8.2598	125.37004	0.5375	8.2598	125.37004	0.54
A70	8.18907	124.88734	0.8756	8.18913	124.88705	0.8521
R72	8.43611	122.47663	0.7356	8.43611	122.47663	0.7214
V73	7.70672	125.46648	1.2246	7.70672	125.46648	1.2242

	[.295mM]			[.3mM]		
Residue	H shift	N shift	Intensity	H shift	N shift	Intensity
M1	8.38926	121.6088	0.313	8.38926	121.6088	0.3086
E2	8.35403	122.18784	0.6197	8.35403	122.18784	0.6301
E3	8.39511	123.51105	0.7253	8.39511	123.51105	0.762
Q5	8.52412	121.02864	0.4647	8.52412	121.02864	0.4538
S6	8.34214	117.75184	0.2244	8.34209	117.75223	0.2294
D7	8.40094	123.63397	0.2585	8.40085	123.63467	0.2633
S9	8.49503	116.01578	0.4404	8.49514	116.01688	0.4473
V10	7.82432	121.12682	0.646	7.82432	121.12682	0.6378
E11	8.30132	126.1895	0.5565	8.30132	126.1895	0.5723

	[.295mM]			[.3mM]		
Residue	H shift	N shift	Intensity	H shift	N shift	Intensity
L14	8.31855	122.57297	0.6617	8.31855	122.57297	0.68
S15	8.28896	116.69362	0.0052	8.28896	116.69362	0.003
S15'	8.35386	116.88319	0.2728	8.35386	116.88511	0.2757
Q16	8.4716	122.57481	0.1396	8.4716	122.57481	0.1375
E17	8.4006	122.08997	0.2074	8.40094	122.06818	0.1988
T18	8.05494	114.79594	0.0018	8.05509	114.79355	-0.0084
T18'	8.39349	113.50728	0.0866	8.39615	113.55131	0.0822
F19	8.21242	122.12473	0.0002	8.21229	122.12437	0.0204
F19'	8.15385	123.1517	0.2032	8.15391	123.15269	0.2062
S20	8.06527	116.6796	0.003	8.0649	116.67986	-0.0082
S20'	7.94943	117.20791	0.1093	7.94951	117.20859	0.1238
D21	8.21766	122.03085	-0.0045	8.21948	122.00103	0.0092
D21'	8.11862	121.41552	0.1091	8.1185	121.41703	0.117
L22	7.90668	121.03059	0.1906	7.9065	121.02936	0.1854
W23	7.81059	119.39096	0.0099	7.81002	119.44991	0.0206
W23'	7.76556	119.39096	0.1014	7.76561	119.39135	0.1059
K24	7.55174	120.45013	-0.0019	7.5583	120.45602	0.0091
K24'	7.30714	120.16318	0.0555	7.30622	120.16345	0.0629
L25	7.78895	120.74191	0.0072	7.78895	120.74191	0.012
L25'	7.88326	120.35471	0.1394	7.88337	120.31641	0.1361
L26	7.87196	123.73206	0.0032	7.87196	123.73206	0.0093
E28	8.67167	119.77691	-0.0029	8.67167	119.77691	0.0018
N29	8.23474	118.80256	0.0585	8.23382	18.80187	0.0552
N29'	8.21282	118.90545	0.1556	8.2125	118.81223	0.1716
N30	8.24799	119.58353	0.0056	8.24799	119.58353	0.0095
V31	7.98919	120.01202	0.2659	7.98919	120.01202	0.2829
D49'	8.03612	119.58424	0.163	8.03623	119.53722	0.1598
L32	8.23262	125.72092	0.0448	8.23262	125.72092	0.05
S33	8.17735	118.04178	0.0159	8.17735	118.04178	0.0158
S33'	8.15383	118.32117	0.252	8.15384	118.28263	0.2321
L35	8.27118	123.63547	0.0195	8.27118	123.63547	0.0223
S37	8.25975	115.34061	0.1064	8.25975	115.34061	0.0973
Q38	8.31953	122.27681	0.0749	8.31953	122.27681	0.0766
A39	8.34804	124.90046	0.0631	8.34804	124.90046	0.0606
A39'	8.20094	124.40679	0.1768	8.20094	124.40679	0.1814
M40	8.2833	119.48781	0.0058	8.2833	119.48781	0.0026
D41	8.21256	121.02966	0.005	8.21256	121.02966	0.0079
D41'	8.1656	120.64322	0.2888	8.16563	120.64493	0.2995
D42	8.20136	120.25745	-0.0048	8.20136	120.25745	0.0038
D42'	8.16556	119.87314	0.3767	8.16556	119.87314	0.3759
L43	8.03618	121.70514	0.0046	8.03618	121.70514	0.0025
L43'	8.00065	121.22326	0.2598	8.00065	121.22326	0.2752
M44	8.20092	120.25786	-0.0048	8.20092	120.25786	0.0038

	[.295mM]			[.3mM]		
Residue	H shift	N shift	Intensity	H shift	N shift	Intensity
L45	8.02303	122.4298	-0.0052	8.02345	122.42769	0.0087
L45'	8.00083	122.57233	0.2279	8.00086	122.57387	0.2302
S46	8.50685	118.33015	0.1887	8.50689	118.33115	0.1901
D48	8.16545	118.7165	0.0161	8.16545	118.7165	0.0198
D49	8.04804	120.16246	0.0018	8.04804	120.16246	-0.005
I50	7.80111	120.16142	0.0019	7.80111	120.16142	-0.0051
I50'	7.75964	119.96877	0.2023	7.75541	119.96957	0.207
E51	8.2952	123.63458	0.0191	8.2952	123.63458	0.0102
Q52	8.09501	120.35492	-0.0096	8.09501	120.35492	-0.0123
W53	7.92757	121.38475	-0.003	7.92757	121.38475	0.0069
F54	7.93004	121.45496	-0.003	7.93004	121.45496	0.0069
T55	7.94187	116.20855	0.0152	7.94187	116.20855	-0.0003
T55'	7.90667	115.62993	0.1718	7.9067	115.63062	0.1835
E56	8.2716	123.34435	0.3508	8.27139	123.34557	0.3566
E56'	8.24799	122.86167	0.1829	8.248	122.76694	0.1887
D57	8.39443	123.38213	0.2868	8.39443	123.38213	0.2877
G59	8.36547	109.33525	0.4917	8.36573	109.31077	0.4965
D61	8.41276	119.96958	0.6638	8.41272	119.97058	0.6792
E62	8.08322	120.8369	0.6073	8.08322	120.8369	0.6072
A63	8.23623	126.62392	0.7873	8.23617	126.62482	0.8044
R65	8.41815	121.89729	0.5597	8.41815	121.89729	0.553
M66	8.43615	123.34467	0.3645	8.43643	123.30646	0.3599
E68	8.50699	121.22407	0.6554	8.50686	121.22396	0.6882
A69	8.2598	125.37004	0.5334	8.25962	125.37114	0.5217
A70	8.18917	124.88806	0.8579	8.18911	124.88896	0.8876
R72	8.43611	122.47663	0.7158	8.43611	122.47663	0.7191
V73	7.70672	125.46648	1.2273	7.70679	125.46768	1.2415

Appendix 4: Paramagnetic Relaxation Enhancement of ^{15}N labeled p53TAD Δ74_72R or p53TAD Δ74_72P.

Residue	Δ74_72P +vitC	Δ74_72P	Δ74_72R + vitC	Δ74_72R
M1	1.2578	0.6775844	1.8563	0.6587072
E2	2.3401	0.6934862	3.3744	0.8120625
E3	3.5797	0.9467852	3.7809	1.0987821
Q5	1.4971	0.545193	2.746	0.6374394
S6	1.2111	0.8257875	1.4666	0.9192558
D7	1.253	0.731978	1.7118	0.6681979
S9	1.9254	0.8421835	2.2862	0.9021456
V10	2.2395	0.8471403	2.6436	0.9128058
E11	2.2239	0.6596761	3.3712	0.7868116
L14	0.4344	0.1960023	2.2163	0.1773865
S15	0.4371	0.3428235	1.275	0.2723837
Q16	0.1257	0.196161	0.6408	
E17	0.36	0.2936858	1.2258	
T18	0.6051	0.4444036	1.3616	0.3404427
F19	0.1892	0.1947504	0.9715	0.1016667
S20	0.0863	0.1759429	0.4905	0.1129371
D21	0.2917	0.3897648	0.7484	0.3184904
L22	0.687	0.3329134	2.0636	0.2409114
W23	0.2064	0.1754058	1.1767	0.061976
K24	0.0821	0.081505	1.0073	0.0720431
L25	0.1274	0.12726	1.0011	0.1198311
L26	0.0131	0.0111641	1.1734	0.0093925
C28	-0.0148	-0.0237294	0.6237	0.0822959
N29	-0.0121	-0.0323184	0.3744	0.088071
N30	0.285	0.2047267	1.3921	0.1288469
V31	0.0937	0.0636246	1.4727	0.14461
L32	0.4034	0.0946304	4.2629	0.0862133
S33	0.0973	0.0829356	1.1732	0.0667964
L35	0.3043	0.1570662	1.9374	0.1211191
S37	0.195	0.2312344	0.8433	0.0713231
Q38	0.1601	0.5080927	0.3151	0.0598381
A39	0.313	0.2471378	1.2665	0.2125896
M40	0.2119	0.688434	0.3078	0.0505548

Residue	Δ74_72P +vitC	Δ74_72P	Δ74_72R + vitC	Δ74_72R
D41	0.6676	0.3735661	1.7871	0.2338333
D42	1.252	0.4143089	3.0219	0.5228571
L43	0.9004	0.3278712	2.7462	0.2717098
M44	0.7781	0.2751025	2.8284	0.14737
L45	0.4043	0.2180455	1.8542	0.0828146
S46	0.6889	0.2670983	2.5792	0.1787442
D48	0.693	0.3990097	1.7368	0.3013642
D49	1.9321	0.7249634	2.6651	0.6892447
I50	1.4681	0.4907079	2.9918	0.4757233
E51	0.344	0.6584992	0.5224	0.1143484
Q52	0.6707	0.3582034	1.8724	0.4323431
W53	0.2851	0.1723596	1.6541	0.1778451
F54	0.8276	0.3763358	2.1991	
T55	0.5489	0.3358008	1.6346	0.305
E56	1.5327	0.5168263	2.9656	0.6020261
D57	0.7742	0.4953295	1.563	0.8352561
G59	2.4075	0.8234992	2.9235	0.9100806
D61	2.5976	0.9051186	2.8699	0.9862021
E62	2.7243	0.988211	2.7568	1.0273684
A63	3.1361	0.9071214	3.4572	0.9280714
R65	1.6871	0.5942167	2.8392	
M66	1.3452	0.6183122	2.1756	0.5537269
E68	2.3047	0.672081	3.4292	0.6971429
A69	2.7567	0.8565702	3.2183	0.6932591
A70	3.1639	0.7421943	4.2629	0.7802326
V73	4.9883	1.036293	4.8136	1.0802083